

8. PETROLOGY AND GEOCHEMISTRY OF BASALTS FROM HOLE 396B, LEG 46

M.F.J. Flower,^{1,2} W. Ohnmacht,¹ H.-U. Schmincke,^{1,3} I.L. Gibson,^{4,5} P.T. Robinson,⁶ and R. Parker⁷

ABSTRACT

Basalts from the upper 255 meters of the oceanic crust at Site 396B show moderately large variations in petrography, mineralogy, and chemistry. The upper part of the section comprises aphyric basalt with rare, rounded plagioclase phenocrysts and lesser amounts of olivine. The central part of the section is olivine and plagioclase phyric with modal abundances ranging from about 10 to 30 per cent. The lowest part of the sequence is moderately phyric with widely varying abundances of olivine and plagioclase phenocrysts. Clinopyroxene phenocrysts occur in only one rock. Co-existing olivine and plagioclase phenocrysts exhibit both normal and reverse zoning which suggests mixing of different magma batches prior to eruption.

Major and trace element compositions of glass and whole rock basalt samples from Hole 396B suggest the following:

a) The two major basaltic magma types are a Ti-poor, Ca-rich ("X") type and Ti-rich, Ca-poor ("Y") type.

b) Different magma batches may represent separate fractions of the same differentiating parent liquid, or may reflect fractionation "events" acting upon similar or distinct liquid compositions. In either case, eruptive products of any one batch show a characteristic chemistry and lithology.

c) Different magma batches appear to have been erupted in a contiguous time sequence except for minor amounts of extreme differentiates interlayered with lavas from unrelated batches. However, eruption of different batches deriving from a single liquid type may be separated by relatively large time intervals.

d) "X"-type and "Y"-type liquids are characterized by different low pressure crystal-liquid phase equilibria. Plagioclase apparently precipitated at higher temperatures compared to olivine and clinopyroxene, for equivalent MgO content in "X"-type than in "Y"-type liquids.

e) Leg 46 basalts generally have higher Na, Ti, and large ion lithophile (LIL) element abundances for equivalent MgO content than basaltic magmas from other parts of the Mid-Atlantic Ridge (e.g., FAMOUS). We tentatively suggest that these differences reflect lower degrees of partial melting at 22°N and are a reflection of ambient geothermal conditions.

INTRODUCTION

Leg 46 of the Deep Sea Drilling Project drilled basaltic basement to a depth of 255 meters at Site 396, located at

22°59.14'N and 43°30.90'W about 150 km east of the axial part of the Mid-Atlantic Ridge (Figure 1). Shipboard studies of the drilled rocks showed significant variations in petrography, mineralogy, and chemical composition; several distinct lithological, chemical, and magnetic units were defined.

We have undertaken a petrographic, mineralogical, and chemical study of selected rocks from the entire stratigraphic section in order to: (1) study the modal and chemical composition of phenocryst phases; (2) identify and characterize compositional groups from glass and whole rock chemical compositions; (3) determine the relationship between whole rock and glass chemistry and the nature and extent of chemical differentiation; (4) study the relation in time of cogenetic (or unrelated) magmas with physical

¹Inst. für Mineralogie der Ruhr-Universität, 463 Bochum, W. Germany.

²Also at Imperial College, London, SW7 2BP, U.K.

³On leave at Department of Geological Sciences, University of California, Santa Barbara, California U.S.A.

⁴Department of Geology, Bedford College, London, NW1, U.K.

⁵On leave at Department of Geology, Dalhousie University, Halifax, Nova Scotia, Canada.

⁶Department of Earth Sciences, University of California, Riverside, California U.S.A.

⁷Department of Geology, Imperial College, London, SW7 2BP, U.K.

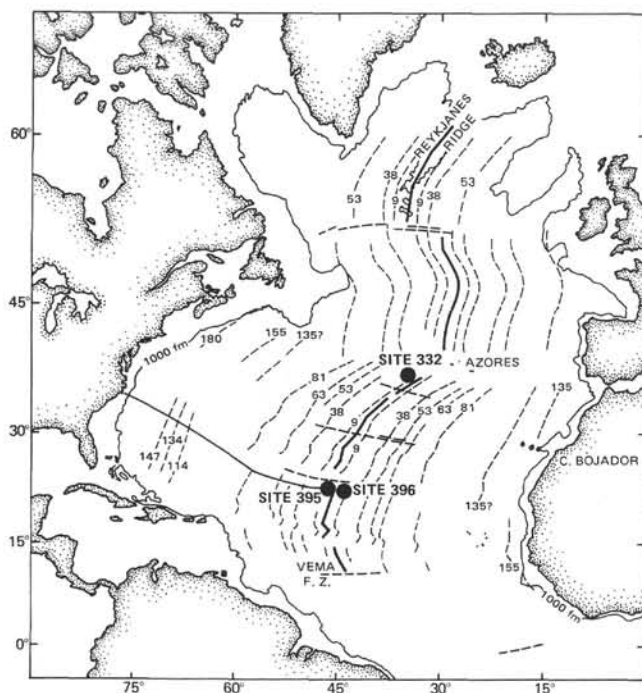


Figure 1. Location map showing Sites 395 and 396 on the Mid-Atlantic Ridge at 22°N, in comparison with Leg 37, Site 332.

characteristics such as magnetic polarity in order to develop constraints on the eruptive, tectonic, and geothermal processes operating at the rift.

Throughout this report, we refer to the analyzed specimens by their Bochum computer file numbers. These Bochum sample numbers are cross-referenced to respective DSDP numbers and approximate sub-bottom depths in Table 1. Thirty microprobe analyses of glassy cooling rinds of pillows, sideromelane breccias, and hyaloclastites are given in Table 2; about 40 analyses for major and trace elements are given in Tables 3 and 4. Sixteen specimens were analyzed for rare earth elements (REE), Th, Ta, and Hf (Table 5). About 40 mineral compositions were determined for phenocryst and groundmass phases (Tables 6 through 8), and modal analyses were made for 14 selected specimens (Table 9).

ANALYTICAL TECHNIQUES

Mineral Analyses

Analyses were performed with an automatic ARL electron microprobe SEMQ with 6 channels (ETH, Zürich). Acceleration voltage was 15 kv, sample current 20 na. K_{α} lines were taken for all elements (Si, Al, Fe, Mg, Ca, Na, K, Ti, Mn, and Cr). Standards used were natural clinopyroxene (for Si, Mg, and Ca), garnet (Al and Fe), labradorite (Na), orthoclase (K), sphene (Ti), chromite (Cr), and a synthetic glass of Mn-garnet composition (Mn). Data reduction was achieved with the aid of program EMMA (ETH, Zürich) which corrects raw microprobe data

TABLE 1
Key to Bochum (lab) Numbers and Methods of Analysis
for Samples From Hole 396B

Bochum Sample No.	Sample (Interval in cm) (Piece No. in parentheses)	Sub-basement Depth (m)	Analysis	Shipboard Chem. Unit
10	4-1, 72-77 (6)	1.99	G	
20	4-1, 80-87 (7A)	2.20	R, G	
50	5-2, 87-93 (9)	10.99	R, M	
60	6-1, 87-89 (11)	21.74	G	
70	7-1, 25-30 (4)	24.28	R	A-1
85	7-1, 50-57 (7)	24.50	R	
90	7-1, 60-62 (8)	25.26	R	
110	7-2, 107-113 (10)	30.99	R	
120	7-2, 127-130 (12)	31.56	R	
140	8-1, 128-135 (14B)	38.29	R	
150	8-2, 3-7 (1)	39.26	G, M	
180	9-1, 75-80 (10)	44.62	R	
210	9-2, 125-128 (16)	50.12	G	
230	10-1, 66-68 (10)	54.33	G	A-2
240	10-1, 70-76 (11)	54.87	G	
260	11-2, 27-33 (3A)	63.68	R, M	
290	13-1, 13-18 (2)	65.53	G	
320	13-2, 28-33 (4)	70.61	G	
400	14-1, 121-127 (9)	77.91	R, G, M	
420	14-2, 31-38 (4A)	79.12	R	
450	14-3, 27-33 (2)	82.82	R, G	
470	15-1, 116-120 (12I)	86.07	R	
500	15-2, 111-115 (2A)	87.99	M	
515	15-2, 120-133 (2C)	87.27	R	A-3
520	15-2, 141-147 (2I)	88.41	R	
530	15-3, 7-15 (2A)	88.64	R	
590	15-4, 132-141 (8A)	92.29	R	
600	15-5, 102-105 (13)	93.85	Mo	
610	15-5, 108-111 (14)	93.93	M	
620	16-1, 97-102 (10F)	97.08	R, M	
630	16-2, 107-113 (9)	102.09	R	
690	16-4, 63-68 (8)	110.02	Mo	
700	16-5, 34-36 (4B)	113.75	R	
710	17-1, 4-7 (1)	117.05	R, Mo	B-1
730	17-2, 43-49 (3)	118.99	R	
750/760	17-3, 108-112 (9)	121.18	R, G, M	
780	18-1, 22-27 (2)	122.87	R, G	
810	20-1, 13-18 (1)	136.18	G	
840	20-1, 35-42 (4A)	136.45	R, Mo	
860/870	20-1, 70-80 (4E)	136.88	G, M, Mo	
880	20-1, 131-132 (5)	137.54	G	
890	20-1, 139-141 (6)	137.65	G, Mo	
910	20-2, 58-67 (5B)	138.50	R, G, M	
930	20-3, 3-10 (1)	139.61	M	
940	20-3, 21-27 (3)	139.82	R, Mo	
970	20-4, 6-7 (1)	141.38	G	
980	20-4, 33-39 (5)	141.73	G, Mo	
1000	20-4, 112-121 (12F)	142.68	G, Mo	
1020	20-5, 60-68 (8)	143.83	R, M, Mo	
1030	20-6, 13-20 (2)	145.04	R, Mo	B-2
1060	21-1, 3-10 (1)	145.78	R, Mo	
1070	21-1, 102-110 (12A)	150.53	R	
1080	21-2, 43-44 (4)	154.67	G	
1090	22-1, 30-38 (5)	155.61	R, Mo	
1100	22-1, 125-134 (14)	157.32	R, G, M	
1110	22-2, 8-12 (1)	157.88	R, Mo	
1140	22-2, 122-144 (7I)	160.00	Mo	
1165	22-3, 28-38 (2A)	160.75	R	
1170	22-3, 49-56 (3A)	161.34	R	
1180	22-3, 92-98 (7A)	162.11	R, Mo	
1190	22-4, 4-9 (1A)	163.21	R	
1200	22-4, 23-26 (3)	163.37	M	
1240	24-1, 15-16 (3)	175.42	G	
1250	24-1, 19-23 (4)	175.99	G	
1280	24-1, 88-90 (14)	182.45	G, M	
1290	25-1, 3-5 (1)	186.67	G	C
1300	28-1, 4-5 (1)	209.87	G	
1350	30-1, 84-86 (1)	231.23	G, M	
1360	32-1, 11-13 (2)	237.09	R, Mo	D
1370	32-1, 59-62 (9)	241.43	R, M, Mo	

Note: R = whole rock chemical composition, G = glass microprobe composition, M = mineral microprobe composition, Mo = modal analysis.

for absorption, fluorescence by characteristic and continuous radiation, backscatter losses, and ionization-penetration losses. Results are believed to be accurate to about 1 to 2 relative per cent for major elements.

Glass Analyses

Glass analyses were performed on an automated MAC model 5-SA3 electron microprobe, Division of Geological and Planetary Sciences, California Institute of Technology, Pasadena. Standards and data reduction are based on a program by A.A. Chodos. Sample current for all analyses was 0.01 μ a and the spot diameter was 30 to 40 μ m. Wherever possible, two or more spots were analyzed for each specimen and the results averaged (Table 2).

Major Element Whole Rock Analyses

Major elements were determined by X-ray fractionation (XRF) methods using a Phillips PW 1410 under the following conditions:

	SiO ₂ , Al ₂ O ₃ , P ₂ O ₅	Fe ₂ O ₃ , K ₂ O	CaO, TiO ₂
Tube		Cr	
Generator	50kv, 30ma	50kv, 30ma	45kv, 18ma
Detector		Flow Counter (1.7kv)	
Path		Vacuum (<0.3 Torr)	
Collimator	Coarse	Fine	Fine
Crystal	PE	LiF (200)	LiF (200)
Line		k α	
Sample holder		Electrolyte-Cu	

Glass discs were prepared of international standards, Leg 46 standards, and Leg 46 rock powders using the following proportions: 5.15 grams LiBO₂ (dried at 550°C, 1 hr.); 0.70 grams La₂O₃ (dried at 900°C, 1 hr.); 1.20 grams rock powder (dried at 1000°C, 2 hr.); and 0.05 grams LiNO₃. All discs were ground and polished before being analyzed. The raw data were corrected for background and drift. Least-squares calibration curves for each oxide were computed using the data of Abbey (1973), multiplied by loss-on-ignition (LOI) factors. LOI was determined on powders dried at 110°C for 24 hours. No corrections were made for Ca-P spectral interferences; however, the error for P is thought to be negligible because unknowns and standards are similar in composition.

Determinations of FeO, Na₂O, MnO, CO₂, and H₂O were done potentiometrically, by AAS, coulometric titration (CTA-5 analyzer), and coulometric Karl-Fischer-titration (AQUATEST-analyzer). The analytical results for three Leg 46 interlab comparison samples are included in Table 3 as Bochum sample numbers 85, 515, and 1165 (DSDP Samples 396B-7-1, 50-57 cm; 15-2, 120-133 cm; and 22-3, 28-38 cm; respectively) along with the other major element data.

Trace Element Whole Rock Analyses (XRF)

The XRF trace element determinations were done on whole rock pressed powder pellets using a Philips 1212 automatic X-ray fluorescence spectrometer. Sr, Rb, and Y were analyzed using a Mo X-ray tube, a LiF₂₂₀ diffraction crystal, and a fine collimator. The remaining trace elements were analyzed using the same diffraction crystal and collimator, and a W X-ray tube. The scintillation and flow proportional counters were used for all elements. The raw

data were processed using a modified form of a computer program supplied by B. Gunn. Corrections were made in this program for dead time, matrix effects (using whole rock major element oxide data), line interference, and X-ray tube spectral contamination.

Three standards (W-I, AGV, and BCR) were analyzed with the samples and the values obtained for these standards are listed in Table 4. This table also lists the values recommended by Flanagan (1973), Abbey (1973), and Willis et al. (1972).

Instrumental Neutron Activation Analyses

The trace elements (Ta, Hf, and Th) and the rare earth elements (Ce, Nd, Eu, Tb, Yb, and Lu) were determined by instrumental neutron activation analysis (Gordon et al., 1968). Accurately weighed powdered rock samples (~0.5 g) were irradiated for 40 hours at a flux of 1×10^{12} n cm⁻² sec⁻¹ at the University of London Reactor Center, Silwood Park, Ascot. After a one-week delay to allow for the decay of interfering short-lived activities, the samples were counted using a planar Ge(Li) 1-cm³ low energy photon detector with a resolution of 640ev at 122kev. The gamma spectra were recorded on a 1028 channel multi-channel analyzer. Data reduction was by means of the photopeak method of Routi and Prussin (1969).

U.S. Geological Survey Standards G2, AGV, BCR, W-1, and GSP-1 were used for primary calibration and the Alisa Craig granite, supplied by the Open University, was used as a radiation standard. Results for two determinations of NIM-G (Table 5) give an indication of the accuracy and precision of the method.

LITHOLOGY AND PETROGRAPHY

Hole 396B penetrated 255 meters into acoustic basement. Recovery averaged about 23 per cent but was much higher in the upper pillowed sequence than in the lower clastic units. Eight lithologic units were defined by the Shipboard Party according to type and abundance of phenocrysts and structural character. Units 1 and 2 are pillow basalts and Unit 3 is a thick flow of very sparsely (<2 modal %) olivine and plagioclase phyric basalt. Unit 4 is highly plagioclase-olivine-spinel phyric basalt and Unit 5 is sparsely plagioclase-olivine phyric pillow basalt. Units 6 and 8 are composed mostly of uncemented clastic deposits ("hyaloclastite") with a thin interlayered pillow zone (Unit 7). These rocks vary from sparsely to moderately olivine and plagioclase phyric. (The "hyaloclastite" is discussed in detail by Schmincke et al., this volume.) Modal analyses of representative samples are given in Table 9 and plotted in Figure 2.

Phenocrysts in shipboard chemical Units B-1, B-2, and C make up 15 to 20 volume per cent with a maximum of about 25 per cent, plagioclase being about 5 to 10 times as abundant as olivine. Sparse spinel occurs as inclusions and single phenocrysts in a few samples and clinopyroxene phenocrysts occur in glomerophytic clusters with plagioclase and olivine in one sample only. Groundmass phases are plagioclase, olivine, and clinopyroxene with glass and oxides. Alteration products are common but generally subordinate and comprise smectite, carbonate, and zeolites. Phenocrysts are generally fresh, although olivine is completely altered in

TABLE 2
Microprobe Analyses (%) of Basalt Glass, Leg 46, Hole 396B (sample current 0.01 μ a, spot diameter 30-40 μ m)

Bochum No.	10	20	60	150	210	230	240	290	320	400	450	750	780	810	870	880	890
Sample (Interval in cm)	4-1, 72-77	4-1, 80-87	6-1, 87-89	8-2, 3-7	9-2, 125-128	10-1, 66-68	10-1, 70-76	13-1, 13-18	13-2, 28-33	14-1, 121-127	14-3, 27-33,	17-3, 108-112	18-1, 22-27	20-1, 13-18	20-1, 70-80	20-1, 131-132	20-1, 139-141
Shipboard Chem. Unit	A-1	A-1	A-1	A-2	A-2	A-2	A-2	A-2	A-3	A-3	A-3	B-1	B-1	B-2	B-2	B-2	B-2
Glass Group	X-1	X-1	X-1	Y-1	Y-1	Y-1	Y-1	Y-1	Y-1	Y-1	Y-2	X-2	X-2	X-2	X-2	X-2	X-2
SiO ₂	50.85	50.58	50.44	50.99	50.48	51.14	50.92	51.09	51.05	50.35	50.18	50.61	50.62	49.81	49.83	50.04	49.52
TiO ₂	1.45	1.42	1.44	1.57	1.56	1.54	1.49	1.50	1.54	1.55	1.71	1.44	1.45	1.42	1.43	1.39	1.38
Al ₂ O ₃	15.01	14.95	15.15	14.99	15.47	14.93	14.78	15.79	15.25	14.98	15.24	15.28	14.82	14.81	14.95	15.65	16.31
FeO*	8.96	9.33	9.18	9.29	9.31	9.43	9.51	9.03	9.59	9.33	10.03	9.51	9.40	9.34	9.35	9.24	9.17
MnO	0.24	0.16	0.17	0.15	0.18	0.16	0.21	0.20	0.18	0.14	0.16	0.13	0.16	0.20	0.16	0.18	0.19
MgO	8.65	8.23	8.33	7.94	8.28	7.53	7.98	7.83	8.04	8.20	7.58	7.93	7.60	7.83	7.70	7.72	7.93
CaO	11.66	11.59	11.45	11.25	11.38	11.34	11.04	10.87	11.24	11.29	10.90	11.58	11.73	11.75	11.90	11.61	11.61
Na ₂ O	2.73	2.79	2.60	2.90	3.00	2.85	2.92	2.80	2.98	2.88	3.24	2.95	2.76	2.82	2.89	2.78	2.80
K ₂ O	0.16	0.12	0.10	0.11	0.13	0.11	0.11	0.13	0.13	0.13	0.09	0.10	0.08	0.11	0.15	0.15	0.09
P ₂ O ₅	0.08	0.13	0.09	0.15	0.25	0.19	0.17	0.18	0.17	0.15	0.21	0.16	0.16	0.09	0.08	0.16	0.13
Cr ₂ O ₃	—	0.04	0.04	0.04	0.07	0.04	0.08	—	0.11	—	—	0.06	—	—	0.05	0.04	—
NiO	—	0.04	—	—	—	—	—	—	0.06	0.04	—	0.07	—	—	—	—	—
BaO	—	—	—	—	—	0.08	0.25	0.25	—	—	—	—	0.18	—	0.10	—	—
SO ₃	0.13	0.13	0.10	0.09	0.17	0.11	0.14	0.08	0.10	0.14	0.14	0.09	0.13	0.11	0.14	0.17	0.12
Total	99.92	99.51	99.09	99.37	100.28	99.45	99.60	99.75	100.44	99.18	99.48	99.91	99.09	98.29	98.73	99.13	99.25
No. of Analyses	1	2	2	2	1	2	2	1	2	1	2	1	3	3	2	2	1

some samples, particularly in the lower part of shipboard chemical Unit B-2 and the upper part of shipboard chemical Unit C (see also Honnorez et al. this volume). Phenocrysts in many rocks exhibit disequilibrium textural features (Plates 1 through 5). For example, plagioclase phenocrysts in rocks of shipboard chemical Unit A are generally rounded; in more phyrlic units, both euhedral and highly resorbed plagioclase and olivine phenocrysts co-exist. Vesicles make up as much as 2 per cent of some rocks and, generally, the most phyrlic rocks also contain the most vesicles. Fresh glass as pillow rinds or clastic shards is common throughout the section.

MINERAL CHEMISTRY

Olivine

About 65 analyses of olivine phenocrysts and a few groundmass crystals were made from 17 samples representing all lithologic units. Phenocryst compositions vary from Fo_{89.6} to Fo_{85.0}. Compositions of groundmass olivine range from Fo₈₆ (Bochum Sample 620; DSDP Sample 396B-16-1, 97-102 cm) to Fo₇₆ (Bochum Sample 500; DSDP Sample 396B-15-2, 111-115 cm). Traces of Ca, Mn, Cr, and Ti are present in the structural formulas, but never exceed 0.5 mole per cent (Table 6). Figure 3 shows a plot of Fo content in olivines versus depth. Both normal and reverse zoning occur in some cases within the same rock. Olivines from shipboard chemical Unit B generally have higher Fo contents and a greater compositional range than those from shipboard chemical Units A and C.

Plagioclase

About 110 analyses of plagioclase phenocrysts and groundmass crystals were made for 17 samples from all lithologic units. Compositional zoning is normal, reverse, or oscillatory (sometimes within the same specimen). Phenocryst compositions range from An₈₃ to An₆₅ and groundmass compositions are between An₆₅ and An₅₀, if An, Ab, K feldspar + Ca(Mg,Fe)Si₃O₈ components = 100 per

cent. Ca was not computed entirely as anorthite component. Figure 4 shows that the Ca(Mg,Fe)Si₃O₈ component is lower for phenocrysts than for groundmass crystals. Within each group, no strong correlation exists: Ca(Mg,Fe)Si₃O₈ is approximately constant for varying An content.

In Figure 3, the ranges for An and Ca(Mg,Fe)Si₃O₈ contents of phenocrysts are plotted versus depth. The mean values for both components yield a perfectly symmetrical distribution (i.e., the higher the An-content, the lower the Ca(Mg,Fe)Si₃O₈ content), a feature also characteristic of the groundmass crystals. The K-feldspar content never exceeds 0.84 mole per cent for either phenocrysts or groundmass crystals.

Clinopyroxene

In Bochum Sample 150 (DSDP Sample 396B-8-2, 3-7 cm), a coarse glomerophytic clot of olivine, plagioclase, and clinopyroxene occurs. From core to rim of a clinopyroxene phenocryst, the following compositions (expressed as structural formulae based on 8 oxygens) were found:

Na	C	Mg	Mg	Fe	Mn	Al	Cr	Al	Si	Ti
0.022	0.796	0.185	0.756	0.129	0.003	0.075	0.037	0.090	1.894	0.014
0.026	0.801	0.185	0.751	0.127	0.005	0.079	0.038	0.091	1.891	0.012
0.024	0.796	0.174	0.769	0.127	0.004	0.069	0.031	0.076	1.916	0.011

Two groundmass clinopyroxene crystals in Bochum Sample 500 (D.S.D.P. Sample 396B-15 -2, 111-115 cm) gave the following:

Na	C	Mg	Mg	Fe	Mn	Al	Cr	Al	Si	Ti
0.032	0.766	0.250	0.530	0.376	0.011	0.081	0.002	0.051	1.880	0.045
0.028	0.755	0.260	0.554	0.362	0.010	0.071	0.002	0.045	1.890	0.043

Analyzed crystals are shown in Plates 1 through 5.

MAJOR ELEMENT CHEMISTRY

Glass

Fresh glasses representing glassy cooling rinds of pillows, sideromelane breccias, and hyaloclastites were sampled from as many shipboard-defined chemical units as possible (A-1, A-2, A-3, B-1, B-2, and C). Analyses of 30 glass samples are given in Table 2 and plotted with depth in Figure 5. For any

TABLE 2 – Continued

910	970	980	1000	1080	1100	1240	1250	1280	1290	1300	1350a	1350b
20-2, 58-67	20-4, 6-7	20-4, 33-39	20-4, 112-121	21-2, 43-44	22-1, 125-134	24-1, 15-16	24-1, 19-23	24-1, 88-90	25-1, 3-5	28-1, 4-5		30-1, 84-86
B-2	B-2	B-2	B-2	B-2	B-2	C	C	C	C	C	C	C
X-2	X-3	X-3	X-3	X-3	X-3	Y-3	Y-3	Y-3	Y-3	Y-3	Z-1	Z-2
50.08	50.12	50.17	50.98	49.80	49.86	49.81	50.55	49.94	49.95	50.43	49.39 ±.37	49.63 ±.40
1.37	1.27	1.26	1.30	1.29	1.24	1.52	1.56	1.59	1.57	1.53	1.52 ±.01	1.43 ±.02
14.86	15.21	15.99	15.25	15.12	15.19	15.50	15.59	15.87	15.51	15.39	16.15 ±.19	16.38 ±.16
9.30	8.97	8.33	8.88	9.01	8.99	9.13	8.96	8.92	9.10	9.25	9.18 ±.08	8.90 ±.10
0.17	0.16	0.13	0.16	0.15	0.17	0.15	0.17	0.21	0.16	0.16	0.15 ±.04	0.14 ±.04
7.95	8.32	8.04	8.05	8.24	8.22	8.08	7.53	7.74	7.75	8.01	8.04 ±.04	8.27 ±.15
11.83	11.90	11.93	11.85	12.01	12.07	11.05	11.31	11.46	11.30	11.10	11.17 ±.02	11.38 ±.06
2.89	2.96	2.67	2.78	2.66	2.73	3.12	2.97	3.05	3.01	2.84	3.08 ±.02	2.98 ±.08
0.10	0.10	0.13	0.13	0.14	0.08	0.21	0.16	0.22	0.21	0.22	0.18 ±.02	0.16 ±.01
0.06	0.14	0.17	0.17	0.16	0.11	0.12	0.19	0.20	0.21	0.19	0.21 ±.08	0.20 ±.04
0.10	0.05	–	–	–	0.10	–	0.07	–	–	0.09	0.06 ±.02	0.07 ±.03
–	–	–	–	–	0.05	–	–	–	–	0.07	–	–
0.17	–	0.22	–	–	0.13	–	–	–	–	–	–	–
0.17	0.12	0.13	0.14	0.17	0.15	0.15	0.13	0.14	0.10	0.14	0.13 ±.03	0.12 ±.03
99.05	99.36	99.17	99.69	98.75	99.09	98.84	99.19	99.34	98.87	99.42	99.26	99.66
1	2	1	2	1	2	2	2	1	2	1	11	6

given MgO content, most variation is shown by TiO₂; there is strong positive and negative covariance, respectively, with FeO and CaO (Figures 6[a] and 6[b]). Based on TiO₂ contents and stratigraphic occurrences, two major glass compositional groupings can be recognized (“X” and “Y” types). These are divided into X-1, X-2, X-3, Y-1, Y-2 (one analysis only), and Y-3 subgroups (Figures 6 and 7). A third major glass group (“Z” type) is recognized in the hyaloclastic unit (Table 2 and Figure 6).

Most oxide contents of Leg 46 glasses range within the spread of data for other regions of the Mid-Atlantic Ridge (e.g., FAMOUS, 36-37°N; Flower et al., 1977a,b) with the exception that TiO₂ and Na₂O are distinctly higher, and CaO is in some cases below the lowest FAMOUS and Leg 37 values for equivalent MgO content. Normative character (CIPW) of the glasses is typical of MORB compositions of “low-K tholeiite” type, and the parameter An/Di, used by Flower et al. (1977, in press) to distinguish magma variants at Leg 37 drill sites, ranges between about 1.1 and 1.6, which spans the range of Leg 37 and FAMOUS glasses.

Although shipboard-defined chemical “units” were established to represent contiguous stratigraphic intervals, there is clearly the possibility that chemically distinct magma types may be interlayered in places. Moreover, different chemical “units” may relate to the same parent liquid and simply reflect varying degrees of fractionation or accumulation prior to eruption.

The glass analyses in Table 2 are annotated according to glass compositional groups and are related to shipboard chemical units as follows:

Liquid Type	Bochum Sample Nos. (Glass)	Shipboard “Unit.”
X-1	10, 20, 60	A-1
X-2	750, 780	B-1
	810, 870, 880, 890, 910	B-2
X-3	870, 980, 1000, 1080, 1100	B-2
Y-1	150, 210, 230, 240, 290, 320	A-2
	400	A-3?

Y-2	450	A-3
Y-3	1240, 1250, 1280, 1290, 1300	C
Z-1,2	1350	C

The stratigraphic distribution of glass (liquid) types (X,Y,Z) confirms the difference between A-1 and A-2 shipboard units, although no samples close to the boundary were analyzed (Figure 5). Shipboard Unit A-2 and the upper part of A-3 correspond to our Y-2 glass group, with a single sample (Bochum Sample 450, DSDP Sample 396B-14-3, 27-33 cm) from shipboard Unit A-3 corresponding to the FeO and TiO₂-rich Y-2 glass type. No glass samples from the top part of shipboard Unit B-1 were studied, but glasses from the lower part are chemically similar to the top part of shipboard Unit B-2, indicating a compositional hiatus within Core 396B-20.

Glass group Y-3 corresponds to shipboard group C. Glasses from the hyaloclastite in Core 396B-30 (Brochum Sample 1350) appear to represent two chemical groups (Z-1, Z-2) somewhat similar to C, but with higher Al₂O₃ and MgO, and lower K₂O and TiO₂. More data are being obtained to precisely define chemical glass groups in this interval.

Whole Rock Samples

To interpret the whole rock chemical data in terms of original magmatic variation, it is necessary to exclude compositions affected by processes of low temperature alteration evidenced by growth of smectite and high contents of H₂O⁺. The presence of fine carbonate veining in many samples also indicates (approximate) stoichiometric addition of CaCO₃ for which correction can be made by subtracting the assumed CO₂-related CaO from the analysis, and normalizing to a H₂O⁺-free basis.

The main chemical effects of low temperature interaction of basalt with seawater appear to be leaching of Ca⁺², oxidation of Fe⁺², and addition of SiO₂, with other effects (such as Mg⁺²-leaching and Fe and Al-enrichment) being associated with more extreme H₂O⁺-related alteration

TABLE 3
Major Element Analyses (%) for Basalts From Hole 396B

Bochum No.	20	50	70	85	90	110	120	140	180	210	260	400	840
Sample (Interval in cm)	4-1, 80-87	5-2, 87-93	7-1, 25-30	7-1, 50-57	7-1, 60-62	7-2, 107-113	7-2, 127-130	8-1, 128-135	9-1, 75-80	9-2, 125-128	11-2, 27-33	14-1, 121-127	20-1, 35-42
Shipboard Chem. Unit	A-1	A-1	A-1	A-1	A-1	A-1	A-1	A-2	A-2	A-2	A-2	A-3	B-2
Magma Batch	1	1	1	1	1	1	1	2	2	2	2	3	4
SiO ₂	49.90	49.85	49.47	49.95	49.93	49.57	49.99	49.97	49.86	49.30	49.99	49.61	49.17
TiO ₂	1.39	1.40	1.39	1.42	1.37	1.38	1.36	1.52	1.54	1.57	1.48	1.62	1.17
Al ₂ O ₃	15.64	15.57	15.86	15.77	15.36	15.53	15.67	15.63	15.68	15.80	15.28	15.43	17.93
Fe ₂ O ₃	2.31	2.83	3.35	2.85	3.34	2.69	2.80	3.34	3.41	3.81	5.69	4.04	3.31
FeO	7.00	6.70	6.20	6.76	5.60	6.70	6.30	6.70	6.70	6.40	4.00	5.90	5.40
MnO	0.16	0.16	0.17	0.17	0.15	0.17	0.16	0.18	0.18	0.18	0.16	0.16	0.15
MgO	7.77	7.91	7.59	8.10	8.05	7.83	8.36	6.93	7.08	7.05	7.57	7.61	6.67
CaO	11.61	11.60	11.81	12.03	11.60	11.60	11.53	11.59	11.55	11.82	11.25	11.06	12.52
Na ₂ O	2.50	2.60	2.50	2.41	2.70	2.50	2.60	2.60	2.70	2.80	2.80	2.90	2.40
K ₂ O	0.18	0.26	0.23	0.22	0.27	0.22	0.25	0.20	0.20	0.16	0.30	0.32	0.18
P ₂ O ₅	0.20	0.20	0.21	0.14	0.17	0.19	0.16	0.18	0.18	0.16	0.20	0.16	0.19
CO ₂	0.19	0.07	0.26	0.06	0.26	0.20	0.19	0.25	0.24	0.21	0.13	0.09	0.10
H ₂ O ⁺	1.10	0.90	1.54	0.63	0.84	1.02	1.00	1.21	1.22	1.10	1.70	1.50	1.26
Total	99.95	100.05	100.58	100.51	99.64	99.60	100.37	100.30	100.54	100.36	100.55	100.40	100.45
H ₂ O ⁻	0.38	0.64	0.71	0.60	1.25	0.60	0.46	0.52	0.55	0.58	1.10	1.12	0.59
L.O.I.	-0.06	-0.20	-0.39	-0.29	-0.73	-0.87	-0.27	-0.28	-0.30	-0.50	-0.71	-0.49	-0.33

reactions (Robinson et al., 1977). We have adopted an empirical value of 1.25 weight per cent H₂O⁺ below which element mobility is taken to be negligible, and accordingly have treated (carbonate-corrected) whole rock analyses by initially projecting their oxide versus MgO variation in terms of the shipboard chemical units, as for the glass data (Figures 8[a], 8[c], 9). This approach is validated by the overall coherence of whole rock major and trace element chemistry. Despite gross compatibility of TiO₂, FeO, and Zr abundances with those of the shipboard chemical units, interpretations in terms of plausible petrologic processes are more complex. Chemical groups with common lithologic character are provisionally interpreted as magma batches, with discrete temporal and spatial identities (cf., Leg 37, Flower et al., 1977, in press). Sampling for chemical analysis from shipboard "units" is summarized as follows:

Shipboard "Unit" No.	Bochum Sample Nos. (whole rocks)	DSDP Sections
A-1	20 to 120	4-1 to 7-2
A-2	140 to 260	8-1 to 11-2
A-3	420 to 590	14-2 to 15-4
B-1	620 to 780	16-1 to 18-1
B-2	840 to 1190	20-1 to 22-4
D	1360, 1370	32-1

We distinguish whole rock compositional groups based on statistical and graphic examination of the major element oxide data in Figure 8. In the following section, we briefly compare these groups to shipboard chemical units in order to understand the eruptive relations of magma batches.

Shipboard Chemical Groups A-1 to A-3: Lithologic Units I, II, and III: Cores 4-1 to 15-4:

Aphyric and sparsely olivine + plagioclase phyrlic pillow basalts from shipboard chemical Units A-1, A-2, and A-3

broadly conform to the chemical characteristics defined on shipboard. We equate them with magma Batches 1, 2, and 3, respectively (Table 3), distinguished largely by differences in TiO₂. The range of TiO₂ content for equivalent Mg/(Mg + Fe⁺²) values of the analyzed whole rock samples are summarized as follows:

Batch No.	Chemical Range	Bochum Sample No. (whole rocks)	Equivalent Shipboard "Unit"
1	TiO ₂ 1.36-1.42%	20, 50, 70 ⁺ , 85, 90, 110, 120	A-1
2	TiO ₂ 1.48-1.57%	140, 180, 210, 260 ⁺	A-2
3	TiO ₂ 1.60-1.65%	400 ⁺ , 420 ⁺ , 450, 470 ⁺ , 515, 520, 530 ⁺ , 590	A-3

+ = "altered" sample (> 1.25% H₂O⁺).

There is no marked compositional gap for CaO between batches, but this element shows marked overall decrease from Batch 1 to Batch 3 with increasing TiO₂ (Figure 10; cf., Y-X liquids in Figure 6[b]). The most significant distinction appears to be that of associated glass type, Batch 1 lavas are related to X-1 liquids, whereas Batches 2 and 3 lavas are probably related to Y-1 and Y-2 liquids, respectively (see Figures 8 and 8[b]).

Shipboard Chemical Groups B-1 and B-2: Lithologic Unit IV: Cores 16-1 to 22-4:

Eruptive units in this interval are much more phyrlic (plagioclase >> olivine) than those discussed above (Figure 2). Examination of oxide versus MgO variation for rocks from shipboard Units "B-1" and "B-2" confirmed several features noted by the shipboard party: (1) Strong Al₂O₃ and CaO enrichment with decreasing MgO, suggesting plagioclase accumulation which is also compatible with the lithology; (2) B-2 rocks generally have higher Al₂O₃ and

TABLE 3 – Continued

1370	420	450	470	515	520	530	590	620	630	700	710	730	750
32-1, 59-62	14-2, 31-38	14-3, 27-33	15-1, 116-120	15-2, 120-133	15-2, 141-147	15-3, 7-15	15-4, 132-141	16-1, 97-102	16-2, 107-113	16-5, 34-36	17-1, 4-7	17-2, 43-49	17-3, 108-112
D	A-3	A-3	A-3	A-3	A-3	A-3	A-3	B-1	B-1	B-1	B-1	B-1	B-1
8	3	3	3	3	3	3	3	4	4	4	4	4	4
49.77	49.65	49.20	49.65	49.69	49.89	49.98	49.93	48.75	49.42	49.77	49.09	49.16	49.08
1.65	1.62	1.65	1.60	1.62	1.61	1.61	1.62	1.16	1.17	1.17	1.20	1.17	1.20
16.21	15.22	15.85	15.20	15.26	15.16	15.19	15.54	17.28	16.40	17.06	17.27	17.34	17.69
3.81	4.67	3.68	4.84	3.32	2.82	3.15	3.09	2.82	3.66	3.34	4.30	2.89	3.12
5.20	5.50	6.70	5.30	6.92	7.20	6.50	6.70	5.60	4.60	4.80	4.70	5.70	5.60
0.16	0.16	0.17	0.16	0.16	0.16	0.16	0.17	0.15	0.13	0.14	0.15	0.15	0.15
6.70	7.39	7.06	7.38	8.02	7.75	7.65	7.65	7.60	7.48	7.18	6.70	7.05	6.83
11.85	10.90	11.06	10.81	10.95	10.81	10.84	11.05	12.16	11.84	12.02	12.40	12.33	12.47
2.70	2.90	2.90	3.00	2.69	2.90	2.80	2.90	2.50	2.60	2.50	2.60	2.50	2.60
0.35	0.33	0.27	0.29	0.14	0.17	0.17	0.19	0.22	0.21	0.24	0.21	0.25	0.13
0.24	0.23	0.21	0.21	0.15	0.22	0.21	0.17	0.17	0.17	0.15	0.13	0.17	0.10
0.46	0.09	0.14	0.10	0.02	0.18	0.22	0.29	0.32	0.21	0.12	0.22	0.30	0.51
1.50	1.40	1.10	1.40	0.79	1.20	1.30	1.20	1.16	1.68	1.53	0.79	1.01	1.15
100.60	100.06	99.99	99.94	99.73	100.07	99.78	100.05	99.89	99.57	100.02	99.76	100.02	100.63
1.09	1.19	0.74	1.21	1.15	0.85	1.06	0.82	0.65	1.10	1.16	1.09	0.62	0.44
-0.81	-0.48	-0.26	-0.79	-0.38	-0.53	-0.63	-0.60	-0.49	-0.97	-0.62	-0.83	-0.53	-0.47

CaO and lower TiO₂, FeO, and Na₂O for equivalent MgO contents than B-1 rocks. However, these gross chemical trends are accompanied by additional features that argue against the implicit postulate of two parallel and analogous trends of plagioclase (± olivine ± clinopyroxene) accumulation, as was demonstrated for Leg 37 rocks (Flower et al., 1977, in press):

1) Al₂O₃ and CaO enrichment trends are accompanied by increases in TiO₂, FeO, and P₂O₅, which are incompatible with the cumulate hypothesis in its simplest form;

2) Within each shipboard unit (B-1 and B-2) distinct magma batches are recognized, separated by small but significant MgO gaps. Also, some B-1 and B-2 analyses overlap for all oxides at a given MgO or Mg/(Mg + Fe⁺²) value.

Hence, we postulate separate magma batches, as for the upper sparsely phyric sequence. These are compatible with trace element data and associated glass compositions and they apparently cross-cut the shipboard B-1/B-2 division, as shown below:

Liquid Batch No.	Liquid (glass) Type	Chemical Range	Bochum Sample No. (whole rocks)	Equivalent Shipboard "Unit"
4	X-2	TiO ₂ 1.61 to 1.20%	620, 630 ⁺ , 700 ⁺ , 710, 730, 750, 840 ⁺ , 910	B-1
5	X-1	TiO ₂ 1.02 to 1.05%	1020 ⁺ , 1030 ⁺ , 1060 ⁺	B-2
6	?	TiO ₂ .92 to 1.03%	1070, 1090 ⁺ , 1100 ⁺ , 1110 ⁺ , 1165, 1170 ⁺ , 1180 ⁺ , 1190	B-2

Oxide variation (Figures 8[a] and 8[c]) of these groups suggests that Batches 4 and 5 are related through simple accumulation of plagioclase ± olivine, as indicated by increases in Al₂O₃ content accompanied by increase in

Mg/(Mg + Fe⁺²) ratios and decreases in TiO₂ and incompatible trace elements (see below). Batch 6, in view of its average Al₂O₃ content being lower than that of Batches 4 and 5, could be tentatively attributed to more extensive accumulation of olivine. However, this is not supported by modal data, and it appears that the significantly higher Mg/(Mg + Fe⁺²) ratio of Batch 6 magmas reflects a more primitive character. Batch 6 does not appear to be related to the X liquid type (the nearest in composition) but probably to a more primitive type for which no glass compositions are known.

Chemical mass balance modeling for the phyric magma batches of whole rock, glass and phenocryst phase compositions, indicates that differentiation of magma batches from any one liquid type is not the result of fractional removal of simple phenocryst phase assemblages, but probably involves interplay of plagioclase accumulation, with accumulation and/or removal of mafic phases and possibly "groundmass" Fe-Ti oxides.

Shipboard Chemical group D: Lithologic Unit VII: Cores 32-1 to 33-1:

Two samples (Bochum Samples 1360 and 1370; DSDP Samples 396B-32-1, 11-13 cm and 59-62 cm) from the lowermost occurrence of shipboard chemical Group D (i.e., from below the clastic sequence) contrast strongly with each other. Bochum Sample 1360 is of the coarsely (plagioclase >> olivine) phyric shipboard chemical Group B rocks with high Al₂O₃ and low TiO₂ (1.28%), but it does not conform exactly in its major or trace element chemistry to any of the batches (4, 5, or 6) that are related to X-type or similar liquids, and so must be provisionally regarded as from a distinct batch (7). Bochum Sample 1370, however, is a high TiO₂ (1.68%) sparsely (olivine + plagioclase) phyric basalt similar to Batch 3 lavas except for higher Al₂O₃ content

TABLE 3 – Continued

Bochum No.	910	940	1020	1030	1060	1070	1090	1100	1110	1165	1170	1180	1190	1360
Sample (Interval in cm)	20-2, 58-67	20-3, 21-27	20-5, 60-68	20-6, 13-20	21-1, 3-10	21-1, 102-110	22-1, 30-38	22-1, 125-134	22-2, 8-12	22-3, 28-38	22-3, 49-56	22-3, 92-98	22-4, 4-9	32-1 11-13
Shipboard Chem. Unit	B-2	B-2	B-2	B-2	B-2	B-2	B-2	B-2	B-2	B-2	B-2	B-2	B-2	D
Magma Batch	4	6	5	5	5	6	6	6	6	6	6	6	6	7
SiO ₂	48.63	49.52	48.36	47.96	48.42	49.76	48.54	48.95	48.57	49.06	48.76	48.90	49.55	48.76
TiO ₂	1.16	1.01	1.02	1.05	1.04	0.99	0.97	0.96	0.92	0.96	0.95	1.00	0.96	1.25
Al ₂ O ₃	17.85	17.48	18.84	18.86	18.33	17.27	18.24	17.67	17.76	17.79	17.39	18.00	17.41	17.63
Fe ₂ O ₃	3.28	2.86	3.83	4.41	4.17	2.52	3.25	2.75	2.39	3.18	2.56	2.89	1.41	3.42
FeO	5.40	4.60	4.10	4.20	4.10	5.20	4.50	4.70	4.90	4.73	5.10	5.20	6.10	5.00
MnO	0.15	0.13	0.14	0.16	0.15	0.14	0.14	0.13	0.13	0.13	0.13	0.13	0.13	0.14
MgO	7.16	7.42	5.86	6.26	6.33	8.24	7.28	7.79	8.44	8.04	8.52	7.84	8.13	6.41
CaO	12.57	12.34	12.47	12.39	12.26	12.15	12.31	12.40	12.04	12.34	12.10	12.36	12.15	12.20
Na ₂ O	2.50	2.50	2.60	2.50	2.60	2.30	2.40	2.40	2.40	2.28	2.30	2.40	2.50	2.80
K ₂ O	0.15	0.20	0.15	0.20	0.17	0.17	0.15	0.22	0.17	0.17	0.19	0.10	0.12	0.27
P ₂ O ₅	0.12	0.14	0.17	0.12	0.19	0.12	0.19	0.16	0.11	0.09	0.13	0.09	0.15	0.19
CO ₂	0.14	0.16	0.26	0.22	0.20	0.11	0.12	0.25	0.11	0.03	0.14	0.09	0.18	0.32
H ₂ O ⁺	0.86	1.56	2.53	2.30	2.66	1.24	2.21	1.91	1.66	0.80	1.60	1.59	1.15	1.05
Total	99.97	99.92	100.33	100.63	100.62	100.21	100.30	100.29	99.60	99.60	99.87	100.59	99.94	99.44
H ₂ O ⁻	0.32	0.94	1.52	1.62	1.65	0.75	1.14	0.94	0.79	1.10	0.72	1.00	0.45	0.49
L.O.I.	-0.51	-0.76	-1.70	-1.77	-1.54	-0.57	-1.21	-1.14	-1.21	-0.77	-1.02	-0.94	-0.44	-0.59

(16.47%). Based on the high Al₂O₃ content (Figure 8[c]), we suggest it may represent yet another separate batch (9).

TRACE ELEMENT CHEMISTRY

Magma batches may also be defined in terms of stable ("alteration-resistant") trace element ratios such as Ti/Zr, Zr/Y, and Ce/Yb. Variation of "mobile" elements (such as Rb and Ba), which are known to be "incompatible" during low pressure fractional crystallization or crystal accumulation processes, may also be used to monitor the extent of low temperature alteration and interaction with seawater. All trace element data obtained by XRF are given in Table 4, whereas REE, Th, Ta, and Hf (determined by INAA) are given in Table 5.

Zr, Y, Sr, and V

Plots of Ti, Y, Sr, and V versus Zr (Figure 11) confirm the chemically distinct magma batches derived from major element data. These elements are plotted in Figure 11 along with average values for chondrite interelement ratios taken from Wänke et al. (1974). It seems likely that the departure from chondrite values of at least some LIL element ratios in both modern and archaic basaltic melt compositions is closely related to residual phase assemblages that characterize progressive degrees of partial melting, especially in view of the close approach to chondrite ratios shown by advanced (about 60 to 70%) komatiitic melts (Nesbit and Sun, 1976), which probably equilibrated with harzburgite or dunite residues.

Ti Versus Zr (Figure 11[a])

The non-cumulate (aphyric) Batch 1 and cumulate Batches 4, 5, and 6 related to X-type liquids, have chondritic Ti-Sr

ratios (~103), whereas Batch 3 (Y-type liquid) has a marginally lower ratio of about 92.

Y Versus Zr (Figure 11[b])

Y vs. Zr variation suggests X-liquid-derived Batches 5 and 6 have an approximately chondritic Y-Zr ratio (~42), whereas a progressive decrease in Y/Zr occurs from X-1, X-4, X-5, and Y-derived batches.

Sr Versus Zr (Figure 11[c])

Aphyric Batch 1 (X-1 liquid) has a Sr/Zr ratio lower than chondrite, whereas the coarsely (plagioclase-olivine) phyrlic Batches 4, 5, and 6 Sr/Zr ratios approximately equal to (Batch 4), or much greater than (Batches 5 and 6), the chondritic value of about 1.8. A progressive decrease in the Sr/Zr ratio is observed from Batch 1 to the sparsely phyrlic Batches 2 and 3, with increasing Zr content.

V Versus Zr (Figure 11[d])

Divergence of V/Zr ratios in all lavas from chondritic values (~13) is far greater than that of other LIL element ratios, although again, we observe a progressive decrease in magma batches from X-3 (~4.2) through to Y (~2.6).

The solid-liquid partition coefficient K_D for Zr in basaltic systems is evidently very low as is that for Ti where oxide phases are not precipitated. The departure from constant element/Zr ratio with increasing Zr content for Y, Sr, and V therefore reflects variable K_D values for these elements with respect to solid phases with which liquids were in contact. It is clear that clinopyroxene is not a major component of low pressure fractionation (evidence from petrography and fractionation calculations), suggesting that clinopyroxene remained in the residue during partial melting, with effective

TABLE 4
Trace Element Data for Leg 46 Rocks and Standards W-1, AGV, and BCR

Comparative Analyses	Elements (ppm)										
	Cr	Ni	Cu	Zn	Zr	Rb	Sr	Y	Ba	V	Co
W-1 Det. ^a Flan. ^b Abbey ^c Willis ^d	118	78	110	84	95	22	192	20	154	244	47
	114	76	110	86	105	21	190	25	160	265	47
	120	78	110	86	105	21	190	25	160	240	50
				95	21	192	20	160			
AGV Det. Flan. Abbey	13	21	60	88	235	67	675	21	1191	125	18
	12	19	60	85	225	68	657	21	1208	125	14
	12	17	64	85	220	68	660	26	1200	125	17
BCR Det. Flan. Abbey Willis	16	11	19	121	188	47	340	33	726	403	37
	18	16	18	120	191	47	330	37	675	400	38
	16	13	19	120	186	46	330	46	680	410	37
	192	47	334	33							
Bochum Sample Number	Elements (ppm)										
	Cr	Ni	Cu	Zn	Zr	Rb	Sr	Y	Ba	V	Co
20	323	139	69	84	78	1	119	29			
30	328	140	65	83	88	<1	124	32		281	
50	312	145				1	119	30		226	
70	302	147	73	86	88	1	121	31		275	42
90	306	150	69	78	86	3	127	31		261	
120	327	186	70	80	84	2	119	29	7	263	
140	286	144	77	90	96	1	129	33		306	44
150	288	131	66	94	98	4	137	34	9	320	
160	321	116	69	98	95	<1	142	33	17	288	
180	268	136	69	90	94	1	128	35	10	303	
210	310	114	65	90	96	<1	134	34		345	
240	285	112				1	138	35		348	
250	268	146	70	87	88	2	125	33		291	42
260	261	141	72	82	94	3	131	32		277	
290	279	136	67	95	101	1	132	34	2	312	133
320	293	135	64	92	93	<1	127	32	4	299	
400	264	172	69	89	104	5	144	35		290	
420	265	162	70	88	111	4	144	34		282	
450	278	150	62	91	110	1	143	36		299	
470	268	160	64	84	110	1	145	35	15	277	
500	239	136	62	84	108	<1	139	35	5	269	38
520	267	139	40	95	610	2	140	35		274	
530	239	143	66	85	112	1	137	35		265	
590	251	154	64	86	110	<1	139	36		276	
610	262	117	69	92	84	2	150	28	18	265	
620	322	143	72	70	72	<1	124	26		242	
630	299	163	73	65	73	1	138	26		228	
700	294	137	66	70	76	2	131	26	19	226	
710	298	140	71	78	73	2	135	28		246	
730	292	129	70	74	72	3	128	28	8	236	
750	313	126	65	79	77	<1	133	29		262	
780	294	151	72	78	74	3	136	27		263	
810	314	156	69	82	76	3	141	27	7	271	
840	296	130	74	75	67	<1	133	26	1	250	37
860	321	139	75	79	72	2	135	27		245	
910	312	140	66	74	71	<1	130	26	15	235	
930	356	137	80	73	67	2	132	27	2	265	65
940	319	167	74	65	60	3	134	23		205	
970	354	125	48	84	60	<1	127	24		251	
1020	334	135	71	74	54	<1	172	24	10	227	
1030	327	154	73	74	57	<1	123	26		227	
1060	355	152	65	77	65	<1	119	25	5	227	
1070	317	167	74	68	56	<1	122	22	201	39	
1090	334	164	67	67	54	1	119	24		203	
1100	339	159	76	64	56	2	123	22		200	
1110	313	180	75	63	50	2	116	22		193	
1170	315	183	73	65	49	2	119	23		204	
1180	321	156					122	23		214	
1190	319	171	69	66	56	<1	119	23		198	
1200	349	164	80	76	54	<1	128	24		237	
1250	327	129	61	81	103	1	168	36	7	342	
1280	292	157	67	85	100	1	165	33	8	296	125
1360	297	145	66	72	88	2	159	27		233	
1370	259	143	65	86	108	4	134	35	5	311	50

Notes: ^aDet. = determined in this work
^bFlan. = Flanagan (1973)
^cAbbey = Abbey (1973)
^dWillis = Willis et al. (1972)

control on both Y ($.5 < K_D^{cpX1} < 1$) and V ($K_D^{cpX1} \approx 1$; Bougault and Hekinian, 1974), at least for those melts that gave rise to X-2, Y-1, and Y-2 liquids. This is probably not a complete explanation, as Y-1 liquid-derived batches have

approximately chondritic Y-Zr ratios but substantially less than chondritic V/Zr ratios.

Similar arguments might be applied to the less than chondritic Sr/Zr ratios of aphyric (Batch 1) and sparsely aphyric (Batches 2 and 3) lavas in postulating residual plagioclase ($K_{Dp1/1} \pm 1$) during generation of parental primary liquids. However this is harder to evaluate as the extent of plagioclase removal from these liquids is clearly very variable.

Cr, Ni, and Co

The "compatible" trace elements ($Kc4D^{s/1} > 1$) show complex patterns of variation versus MgO (e.g., Figure 12 showing Cr versus MgO). Any specific magma batch appears to have a characteristic range of Cr for a given range of MgO, with Cr/Mg showing a rough correlation with Mg/(Mg + Fe⁺²) ratios. The most probable, and simplest, explanation for the variable Cr/Mg character of different magma batches is the variable extent of plagioclase ± olivine accumulation imposed on the spectrum of parent liquid composition.

Rare Earth Elements (REE), Th, Ta, and Hf

Sixteen samples representing all shipboard chemical units except C were analyzed for these elements. The analyses, with chondrite-normalized Ce/Yb ratios, identified according to magma batch, are given in Table 5. The chondrite-normalized distribution patterns for Ce, Nd, Eu, Tb, Yb, and Lu are shown in Figure 13 for each magma batch. The REE configurations for each batch are virtually indistinguishable, except for slight positive Eu anomalies in plagioclase-phyric Batches 5, 6, and 7. All patterns are light REE depleted compared to "typical" mid-ocean ridge basalts.

Magma batches are characterized by the sum of REE abundance \sum Ce, Nd, Tb, Yb, and Lu (see Table 5), coarsely aphyric lavas having lowest abundances (Figure 13[h]). However, REE abundances in aphyric and sparsely-phyric Batches 1, 2, and 3 show an overall inverse correlation with phenocryst abundance (as for Ti and other LIL elements), suggesting higher abundances in Y than in X-type liquids. The uniformity of (Ce/Yb)_N for all magma types is in striking contrast to the variable patterns of Leg 37 basalts, which correlate with other trace element parameters (e.g., Zr/Y) and with magma types defined from a major element chemistry.

WHOLE ROCK-GLASS RELATIONS

Certain provisional interpretations of whole rock-glass relations are briefly summarized below:

a) Glass (liquid) compositions are always more MgO-rich and have higher Mg/(Mg + Fe⁺²) ratios than the bulk compositions of cooling units with which they are associated. This suggests the likelihood that mafic cumulates (essentially olivine) exist which either were not erupted or simply were not encountered during drilling. Liquid compositions are all evolved compared to likely primary melt compositions. However, the plagioclase-cumulate batch magmas have primitive Mg/(Mg + Fe⁺²) ratios in the range of 0.68 to 0.72. These basalts have no glass equivalents.

TABLE 5
Rare Earth Elements and Th, Ta, and Hf Concentrations (ppm) of Samples From Hole 396B, and of Standards

Bochum No.	70	110	120	140	250	420	450	500	530	560	630	690	840	1030	1070	1370			
Sample (Interval in cm)	7-1, 25-30	7-2, 107-113	7-2, 127-130	8-1, 128-135	11-1, 104-108	14-2, 31-38	14-3, 27-33	15-2, 111-115	15-3, 7-15	15-4, 13-20	16-2, 107-113	16-4, 63-68	20-1, 35-42	20-6, 13-20	21-1, 102-110	32-1, 59-62			
Shipboard Chem. Unit	A-1	A-1	A-1	A-2	A-2	A-3	A-3	A-3	A-3	A-3	B-1	B-1	B-2	B-2	B-2	D			
Magma Batch	1	1	1	2	2	3	3	3	3	3	4	4	4	6	5	8	Standards	NIM-G	NIM-G
Ce	9.71	9.05	9.11	10.61	10.31	12.48	13.08	11.52	12.81	12.16	8.0	7.75	7.37	7.0	6.51	11.66		208.69	212.96
Nd	9.46	9.21	8.58	10.51	10.44	11.89	11.08	12.03	10.88	11.67	7.44	8.37	7.33	6.94	6.65	10.87		77.21	83.41
Eu	1.31	1.26	1.17	1.42	1.39	1.54	1.98	1.50	1.47	1.52	1.15	1.18	1.10	1.00	1.00	1.47		0.36	0.33
Tb	0.82	0.82	0.74	0.93	0.90	0.96	0.88	0.95	0.91	0.96	0.70	0.78	0.63	0.61	0.59	0.96		2.87	2.92
Yb	3.38	3.24	2.99	3.76	3.52	3.65	3.25	3.82	3.65	3.8	2.57	2.89	2.58	2.43	2.28	3.77		15.13	15.34
Lu	0.55	0.54	0.51	0.60	0.58	0.57	0.59	0.65	0.59	0.60	0.46	0.48	0.41	0.39	0.37	0.59		2.14	1.76
Th	0.16	0.14	n.d.	0.23	0.21	n.d.	n.d.	0.16	n.d.	0.25	n.d.	0.18	0.16	n.d.	0.14	0.22		56.45	58.36
Ta	0.16	0.15	1.23	0.21	0.18	0.70	1.53	0.21	0.88	0.20	1.04	0.15	0.13	0.63	0.13	0.23		4.49	4.97
Hf	2.54	2.42	2.10	2.75	2.72	3.20	1.16	2.90	3.14	2.94	n.d.	2.11	1.97	1.57	1.66	2.92		12.72	13.11
$\frac{Ce}{Yb+N}$	0.73	0.71	0.77	0.72	0.74	0.87	1.0	0.77	0.89	0.81	0.80	0.68	0.73	0.73	0.72	0.79		-	-

b) Mass balance solutions for glass-whole rock fractionation, in terms of analyzed phenocrysts (\pm Fe-Ti oxides), can in no case be satisfactorily achieved by simple removal or addition of a phase assemblage. Only by postulating the addition of plagioclase and removal of olivine (\pm clinopyroxene \pm Ti-magnetite) can "daughter" whole-rocks be derived from associated "parent" glass compositions. This suggests that either the fractionation processes in the magma storage region are complex or that other processes, such as magma mixing, have affected magma chemistry.

c) As noted previously, glasses associated with sparsely phyric basalts of Batch 1 (X-2 type) are indistinguishable from those associated with the phyric basalts (up to about 30% phenocrysts) of Batches 4 and 5 magmas. Intraunit glass-whole rock fractionation in the latter groups is considerably more extensive and distinctive. This must indicate efficient separation of liquid and crystals for any one liquid type so that the liquid fraction in non-cumulate regions of the storage reservoir remains essentially in equilibrium with that in adjacent cumulate regions.

d) There is an important difference in the nature of glass-whole rock fractionation, between X-type and Y-type liquids. Although both X and Y-type liquids precipitated mafic phases which separated out; X-type liquids gave rise to rocks with higher Al_2O_3 and lower TiO_2 contents than the parent glass. Y-type liquids resulted in lavas, considerably less phyric, showing a similar but less extensive enrichment of Al_2O_3 , but higher TiO_2 contents than those in the glass. As a preliminary conclusion, we suggest this reflects critical differences in the phase equilibria of X and Y-type liquids that are responsible for diversification of lithology and chemical fractionation patterns in Leg 46 basalts, and may also reflect differential movement of "groundmass" Ti-magnetite.

SUMMARY

At least four and probably five magma types were available for eruption during crustal formation at Site 396, each apparently resulting from a specific fractionation event. However, any one eruptive batch of liquid or liquid + crystal mix does not necessarily derive from a single fractionation event. We envisage that magma batches deriving from any one liquid type reflect one or more of several possibilities: (a)

Sampling specific fractions of a magma body differentiating under temporarily closed system conditions. (b) Spatially and/or temporally distinct fractionation events, each characterized by a specific duration, cooling history, and extraction efficiency during an eruptive pulse. (c) An open-ended magmatic system wherein successive magma pulses intrude into and mix with solid and liquid fractionation products of each other. Despite the a priori likelihood of this process, the apparent clustering of both glass and whole rock chemistry and preliminary quantitative interpretations of the variance indicates this could be only a contributing factor.

At this stage of our interpretation, we prefer the first possibility as the dominant influence. Providing that separation of crystal and liquid phases is efficient (i.e., no intra-cumulus "fraction" develops), this represents the simplest explanation of the relation between chemically distinct magma batches and remarkably homogeneous glass compositions. The complex zoning of phenocrysts could be related to a variety of factors and must be reconciled with any final petrogenetic model.

ACKNOWLEDGMENTS

Our work was supported by grants (Schm 250116) from the Deutsche Forschungsgemeinschaft. We thank V. Trommsdorff for permission to use the microprobe at the Institute für Kristallographie, ETH Zürich, and M. Sammerauer for help in operating the instrument. We also thank A. Albee for permission to use the California Institute of Technology microprobe and A.A. Chodos for his assistance. The manuscript was written while H.U. Schmincke was supported by a stipend from the VW Foundation.

REFERENCES

- Abbey, S., 1973. Studies in "Standard Samples" of silicate rocks and minerals, *Geol. Surv. Canada, Paper 73-76*.
- Bougault, H. and Hekinian, R., 1974. Rift valley in the Atlantic Ocean near 36°51'N: petrology and geochemistry of basaltic rocks, *Earth Planet. Sci. Lett.*, v. 27, p.
- Flanagan, F.J. 1973. 1972 values for international geochemical reference samples, *Geochim. Cosmochim. Acta.*, v. 37, p. 1189-1200.
- Flower, M.F.J., Robinson, P.T., Schmincke, H.-U., and Ohnmacht, W., 1977. Petrology and geochemistry of igneous rocks. In Aumento, F., Melson, W.G., et al., *Initial Reports of the Deep Sea Drilling Project*, v. 37: Washington (U.S. Government Printing Office), p. 658-680.

TABLE 6
Structural Formulas (%) of Leg 46 Olivines on the Basis of 4 Oxygens

Bochum No.	Point	Na	K	Ca	Mg	Fe ²⁺	Mn	Cr	Al	Ti	Si	Remarks
50	119	0.0	tr.	0.007	1.741	0.273	0.004	0.001	0.001	0.0	0.985	Fo 86.4 Core
	120	0.0	0.0	0.008	1.745	0.273	0.004	0.0	0.0	0.0	0.985	Fo 86.5 Rim
	121	0.0	0.0	0.007	1.747	0.269	0.005	0.0	0.001	0.0	0.985	Fo 86.7
	122	0.0	0.0	0.008	1.745	0.262	0.004	0.0	0.0	0.0	0.990	Fo 86.9
150	2	0.001	0.0	0.007	1.712	0.283	0.005	0.0	0.0	0.0	0.996	Fo 85.8 Rim
	4	0.0	0.0	0.008	1.700	0.281	0.005	0.002	0.005	0.0	0.998	Fo 85.8 Rim
	3	0.0	0.0	0.008	1.710	0.286	0.005	0.0	0.0	0.0	0.995	Fo 85.7 Core
	12	0.0	0.0	0.008	1.729	0.269	0.004	0.0	0.0	0.0	0.995	Fo 86.5
260	16	0.0	0.0	0.008	1.694	0.300	0.005	0.0	0.0	0.0	0.996	Fo 85.0 Core
	17	0.0	0.0	0.008	1.719	0.298	0.005	0.0	0.0	0.0	0.985	Fo 85.2
	18	0.0	0.0	0.008	1.692	0.297	0.004	0.0	0.0	0.0	1.000	Fo 85.1
	19	0.0	0.0	0.007	1.694	0.294	0.005	0.0	0.0	0.0	1.000	Fo 85.2 Rim
	20	0.0	0.0	0.008	1.706	0.287	0.005	0.0	0.0	0.0	0.997	Fo 85.6 Core
	21	0.001	0.0	0.008	1.716	0.282	0.004	0.0	0.0	0.001	0.994	Fo 85.9 Rim
	25	0.0	0.0	0.008	1.725	0.289	0.005	0.0	0.0	0.0	0.987	Fo 85.7
400	194	0.0	0.0	0.008	1.710	0.299	0.005	0.001	0.0	0.0	0.988	Fo 85.1 Core
	195	0.0	0.0	0.008	1.708	0.294	0.005	0.0	0.0	0.001	0.992	Fo 85.3 Core
	196	0.0	0.0	0.008	1.720	0.296	0.004	0.0	0.0	0.0	0.986	Fo 85.3 Core
500	130	0.0	0.0	0.009	1.623	0.386	0.006	0.0	0.0	0.0	0.988	Fo 80.8 Groundmass
	132	0.0	0.0	0.008	1.510	0.484	0.009	0.0	0.0	0.007	0.987	Fo 75.7 Groundmass
610	140	0.001	0.0	0.008	1.712	0.286	0.005	0.003	0.002	0.002	0.988	Fo 85.7
	141	0.0	0.0	0.008	1.719	0.286	0.005	0.0	0.0	0.0	0.991	Fo 85.7
620	16	0.0	0.0	0.008	1.773	0.249	0.004	0.001	0.0	0.0	0.982	Fo 87.7 Core
	17	0.0	0.0	0.008	1.776	0.253	0.004	0.002	0.0	0.0	0.978	Fo 87.5 Rim
	28	0.0	0.0	0.008	1.765	0.243	0.004	0.0	0.0	0.0	0.990	Fo 87.9 Core
	29	0.0	0.0	0.008	1.772	0.242	0.004	0.0	0.0	0.0	0.987	Fo 88.0
	30	0.0	0.0	0.008	1.780	0.247	0.005	0.0	0.0	0.0	0.980	Fo 87.8 Rim
	32	0.0	0.0	0.008	1.733	0.275	0.004	0.002	0.001	0.0	0.987	Fo 86.3 Groundmass
750/760	64	0.0	0.0	0.008	1.749	0.261	0.004	0.0	0.0	0.0	0.988	Fo 87.0 Close to core
	65	0.0	0.0	0.008	1.755	0.269	0.004	0.0	0.001	0.001	0.980	Fo 86.7 Rim
	66	0.0	0.0	0.008	1.757	0.252	0.004	0.0	0.001	0.0	0.989	Fo 87.5
	73	0.0	0.0	0.008	1.759	0.247	0.005	0.002	0.0	0.0	0.989	Fo 87.7
810	38	0.0	0.0	0.008	1.797	0.211	0.003	0.001	0.0	0.0	0.989	Fo 89.5
	39	0.0	0.0	0.008	1.744	0.268	0.004	0.002	0.0	0.0	0.987	Fo 86.7
860/870	48	0.0	0.0	0.008	1.770	0.247	0.003	0.0	0.001	0.0	0.984	Fo 87.8 Core
	49	0.0	0.0	0.008	1.770	0.249	0.003	0.0	0.0	0.0	0.985	Fo 87.7
	50	0.0	0.0	0.008	1.737	0.269	0.004	0.0	0.0	0.0	0.991	Fo 86.6 Rim
	51	0.0	0.0	0.008	1.762	0.248	0.004	0.0	0.0	0.0	0.989	Fo 87.7
	52	0.0	0.0	0.008	1.741	0.248	0.003	0.0	0.002	0.0	0.998	Fo 87.5 Close to core
	53	0.0	0.0	0.008	1.744	0.265	0.004	0.0	0.001	0.0	0.989	Fo 86.8 Rim
	54	0.0	0.0	0.008	1.789	0.227	0.003	0.0	0.003	0.0	0.984	Fo 88.7 Core
	55	0.0	0.0	0.008	1.776	0.241	0.003	0.0	0.0	0.0	0.986	Fo 88.1 Rim
910	206	0.008	0.0	0.008	1.751	0.245	0.004	0.009	0.010	0.0	0.980	Fo 87.7 Rim
	207	0.0	0.0	0.008	1.769	0.245	0.004	0.001	0.0	0.0	0.986	Fo 87.8 Core
	210	0.0	0.0	0.008	1.771	0.238	0.004	0.0	0.0	0.0	0.990	Fo 88.2
930	159	0.0	0.0	0.008	1.792	0.223	0.005	0.0	0.0	0.0	0.986	Fo 88.9 Core
	160	0.0	0.0	0.008	1.801	0.229	0.004	0.0	0.001	0.0	0.987	Fo 88.7 Rim
	167	0.006	0.001	0.007	1.786	0.208	0.005	0.008	0.010	0.0	0.982	Fo 89.6 Core
	168	0.0	0.0	0.007	1.794	0.211	0.003	0.001	0.001	0.001	0.990	Fo 89.5
	169	0.002	0.0	0.008	1.796	0.222	0.004	0.002	0.003	0.0	0.981	Fo 89.0 Rim
	170	0.0	0.0	0.007	1.762	0.261	0.004	0.0	0.0	0.0	0.983	Fo 87.1 Core
	171	0.0	0.0	0.008	1.761	0.258	0.004	0.0	0.001	0.0	0.983	Fo 87.2 Rim
	172	0.0	0.0	0.007	1.782	0.232	0.004	0.0	0.0	0.0	0.987	Fo 88.5 Core
1020	211	0.0	0.0	0.008	1.768	0.233	0.004	0.002	0.003	0.002	0.987	Fo 88.4 Inclusion plag
1100	187	0.001	0.0	0.008	1.777	0.241	0.004	0.002	0.002	0.001	0.981	Fo 88.1 Small pheno
	188	0.001	0.0	0.008	1.770	0.240	0.004	0.001	0.0	0.0	0.988	Fo 88.1 Small pheno
	189	0.002	0.0	0.007	1.783	0.219	0.004	0.001	0.0	0.0	0.992	Fo 89.1 Small pheno
	190	0.0	0.0	0.007	1.766	0.240	0.004	0.0	0.002	0.0	0.990	Fo 88.0 Core
	191	0.0	0.0	0.008	1.767	0.238	0.004	0.0	0.0	0.0	0.992	Fo 88.1 Rim
1200	28	0.0	0.0	0.008	1.781	0.225	0.004	0.001	0.001	0.0	0.989	Fo 88.8 Core
	29	0.0	0.0	0.008	1.769	0.232	0.005	0.0	0.0	0.0	0.993	Fo 88.4 Rim
	40	0.0	0.0	0.009	1.751	0.246	0.004	0.0	0.001	0.0	0.994	Fo 87.7
1280	60	0.0	0.0	0.007	1.740	0.267	0.005	0.0	0.001	0.0	0.990	Fo 86.7 Core
	61	0.0	0.0	0.008	1.750	0.262	0.004	0.001	0.0	0.0	0.987	Fo 87.0 Rim
	62	0.0	0.0	0.008	1.748	0.263	0.004	0.002	0.002	0.001	0.984	Fo 86.9
1370	41	0.0	0.0	0.009	1.718	0.299	0.004	0.0	0.0	0.002	0.983	Fo 85.2
	43	0.001	0.0	0.008	1.726	0.283	0.004	0.003	0.003	0.001	0.984	Fo 85.9

- Flower, M.F.J., Robinson, P.T., Schmincke, H.-U., Ohnmacht, W., in press. Magma fractionation systems beneath the Mid-Atlantic Ridge at 36-37°N, *Contrib. Mineral., Petrol.*
- Gordon, G.E., Randle, K., Goles, G.G., Corliss, J.B., Beeson, M.H., and Oxley, S.S., 1968. Instrumental activation analysis of standard rocks with high resolution X-ray detectors, *Geochim. Cosmochim. Acta*, v. 32, p. 369-396.
- Nesbit, R.W. and Sun, Sh.-S., 1976. Geochemistry of Archaean spinifex-textured peridotites and magnesian and low-magnesian tholeiites, *Earth Planet. Sci. Lett.*, v. 31, p. 433.
- Robinson, P.T., Flower, M.F.J., Schmincke, H.-U., and Ohnmacht, W., 1977. Low temperature alteration of oceanic basalts, DSDP Leg. In Aumento, F., Melson, W.G., et al.,

- Initial Reports of the Deep Sea Drilling Project*, v. 37: Washington (U.S. Government Printing Office), p. 775-794.
- Routti, J.T. and Prussin, S.G., 1969. Photopeak method for the computer analysis of γ -ray spectra from semiconductor detectors, *Nucl. Instrum. Methods*, v. 72, p. 125-142.
- Wänke, H., Baddenhausen, H., Palms, M., and Spettel, B., 1974. On the chemistry of the Allende inclusions and their origin as high temperature condensates, *Earth Planet. Sci. Lett.*, v. 23, p. 1.
- Willis, J.P., Erlank, A.J., Gurney, J.J., Theil, R.H., and Ahrens, L.H., 1972. Major, minor and trace element data from some Apollo 11, 12, 14 and 15 samples, *Third Lunar Sci. Conf. Proc. Geochim. Cosmochim. Acta*, Suppl. 3, v. 2, p. 1269-1273.

TABLE 7
Structural Formulas (%) of Leg 46 Clinopyroxenes on Basis of 6 Oxygens

Bochum No.	Point	Na	Ca	Mg	Fe ²⁺	Mn	Al	Cr	Ti	Si	Remarks
150	13	0.022	0.796	0.941	0.129	0.003	0.166	0.037	0.014	1.894	Core
	14	0.026	0.801	0.936	0.127	0.005	0.170	0.038	0.012	1.891	
	15	0.024	0.796	0.943	0.127	0.004	0.145	0.031	0.011	1.916	Rim
500	129	0.032	0.766	0.780	0.376	0.011	0.132	0.002	0.045	1.880	Groundmass cryst.
	131	0.028	0.755	0.814	0.362	0.010	0.117	0.002	0.043	1.890	Groundmass cryst.

TABLE 8
Structural Formulas (%) of Leg 46 Plagioclases Based on 8 Oxygens

Bochum No.	Point	K	Na	Ca	Mg	Fe ²⁺	Mn	Ti	Cr	Al	Si	Remarks
50	115	0.002	0.266	0.739	0.012	0.013	0.0	0.0	0.0	1.622	2.334	Core
	116	0.002	0.271	0.755	0.015	0.014	0.0	0.0	0.0	1.636	2.313	
	117	0.002	0.275	0.729	0.016	0.014	0.0	0.0	0.0	1.614	2.341	
	118	0.002	0.287	0.734	0.015	0.015	0.0	0.0	0.0	1.622	2.330	Rim
	123	0.002	0.332	0.675	0.031	0.036	0.0	0.0	0.0	1.531	2.398	Groundmass
	124	0.002	0.357	0.642	0.026	0.031	0.0	0.0	0.0	1.532	2.412	Groundmass
150	5	0.001	0.272	0.743	0.014	0.016	0.0	0.0	0.0	1.621	2.330	Rim
	6	0.001	0.314	0.687	0.019	0.013	0.0	0.002	0.0	1.574	2.379	
	7	0.001	0.321	0.696	0.017	0.015	0.0	0.002	0.0	1.585	2.365	
	8	0.002	0.311	0.710	0.016	0.014	0.0	0.0	0.0	1.614	2.341	
	9	0.002	0.319	0.689	0.016	0.014	0.0	0.002	0.0	1.575	2.377	Core
260	22	0.008	0.289	0.701	0.022	0.046	0.0	0.0	0.0	1.546	2.381	Later
	23	0.004	0.379	0.616	0.028	0.039	0.0	0.014	0.0	1.489	2.432	Groundmass
	24.1	0.002	0.351	0.666	0.027	0.038	0.0	0.004	0.0	1.507	2.412	same point,
	24.2	0.002	0.352	0.666	0.028	0.038	0.0	0.004	0.0	1.512	2.407	different corrections
400	191	0.001	0.215	0.798	0.012	0.014	0.0	0.0	0.0	1.691	2.265	Core
	192	0.001	0.225	0.792	0.012	0.014	0.0	0.0	0.0	1.685	2.270	
	193	0.001	0.192	0.831	0.013	0.016	0.0	0.0	0.0	1.729	2.225	Rim
	197	0.003	0.384	0.609	0.030	0.045	0.0	0.002	0.0	1.471	2.455	Grd. M. (\pm Matrix)?
500	125	0.002	0.462	0.555	0.010	0.032	0.002	0.003	0.0	1.441	2.501	Groundmass
	126	0.002	0.370	0.650	0.020	0.035	0.001	0.006	0.0	1.509	2.416	Groundmass
	127	0.003	0.454	0.548	0.011	0.035	0.0	0.003	0.002	1.432	2.511	Groundmass
	128	0.002	0.424	0.602	0.016	0.026	0.0	0.003	0.002	1.481	2.456	Groundmass
610	133	0.0	0.227	0.784	0.017	0.015	0.0	0.0	0.0	1.675	2.279	Core
	134	0.0	0.248	0.746	0.018	0.014	0.0	0.003	0.0	1.641	2.315	
	135	0.001	0.265	0.759	0.019	0.017	0.0	0.005	0.0	1.624	2.313	same point, different
	136	0.001	0.250	0.753	0.017	0.017	0.0	0.001	0.0	1.652	2.303	
	137	0.001	0.256	0.752	0.017	0.015	0.0	0.003	0.0	1.619	2.327	
	138	0.001	0.270	0.756	0.019	0.019	0.0	0.012	0.0	1.628	2.303	
	139	0.001	0.257	0.753	0.017	0.015	0.0	0.002	0.0	1.632	2.317	Rim
	142	0.001	0.306	0.702	0.024	0.021	0.0	0.018	0.0	1.577	2.349	Small pheno
	143	0.001	0.300	0.712	0.019	0.021	0.0	0.001	0.00	1.584	2.359	Small pheno

TABLE 8 - Continued

Bochum No.	Point	K	Na	Ca	Mg	Fe ²⁺	Mn	Ti	Cr	Al	Si	Remarks
	144	0.001	0.247	0.766	0.017	0.010	0.0	0.0	0.0	1.645	2.307	Core
	145	0.002	0.244	0.787	0.014	0.010	0.004	0.0	0.013	1.646	2.286	Rim
	148	0.001	0.249	0.756	0.018	0.014	0.0	0.0	0.0	1.643	2.312	Small pheno
620	18	0.001	0.254	0.733	0.019	0.018	0.0	0.002	0.0	1.627	2.330	Rim
	19	0.001	0.227	0.775	0.017	0.013	0.001	0.0	0.0	1.685	2.277	Core
	20	0.001	0.202	0.798	0.016	0.011	0.001	0.0	0.0	1.709	2.254	Core
	21	0.001	0.248	0.761	0.019	0.015	0.001	0.0	0.0	1.673	2.284	Rim
	22	0.001	0.222	0.795	0.015	0.014	0.002	0.0	0.0	1.698	2.257	Core
	23	0.001	0.263	0.729	0.017	0.015	0.0	0.0	0.0	1.635	2.328	
	24	0.0	0.240	0.768	0.015	0.016	0.0	0.0	0.0	1.646	2.306	Rim
	25	0.001	0.213	0.795	0.018	0.013	0.0	0.0	0.0	1.707	2.253	Core
	26	0.001	0.192	0.814	0.016	0.013	0.0	0.0	0.0	1.744	2.222	
	27	0.0	0.163	0.840	0.016	0.014	0.0	0.0	0.0	1.757	2.207	Rim
	31	0.001	0.266	0.739	0.019	0.022	0.0	0.0	0.0	1.618	2.330	Groundmass
750/760	67	0.001	0.195	0.803	0.015	0.014	0.0	0.002	0.0	1.709	2.252	Core
	68	0.001	0.164	0.844	0.012	0.015	0.0	0.003	0.0	1.746	2.210	
	69	0.001	0.260	0.751	0.015	0.019	0.0	0.003	0.0	1.641	2.310	Rim
	70	0.001	0.252	0.761	0.017	0.014	0.0	0.0	0.0	1.650	2.304	Core
	71	0.001	0.263	0.743	0.015	0.013	0.0	0.0	0.0	1.641	2.378	
	72	0.002	0.232	0.775	0.014	0.016	0.002	0.0	0.013	1.689	2.261	Outermost Rim
	74	0.001	0.239	0.760	0.017	0.017	0.0	0.002	0.0	1.667	2.290	Pheno
	75	0.002	0.300	0.694	0.022	0.028	0.0	0.003	0.0	1.573	2.370	Groundmass
810	33	0.0	0.248	0.756	0.016	0.012	0.0	0.0	0.0	1.636	2.319	Core
	34	0.0	0.241	0.772	0.015	0.014	0.0	0.0	0.0	1.666	2.291	
	35	0.0	0.230	0.773	0.015	0.015	0.0	0.0	0.0	1.688	2.275	Rim
	36	0.0	0.223	0.775	0.091	0.011	0.0	0.0	0.0	1.682	2.280	Core
	37	0.0	0.189	0.803	0.017	0.013	0.0	0.0	0.0	1.717	2.248	Rim
	40	0.001	0.251	0.760	0.019	0.022	0.0	0.003	0.0	1.640	2.304	Minute later
860/870	42	0.0	0.151	0.864	0.014	0.018	0.0	0.0	0.0	1.776	2.182	Rim
	43	0.0	0.160	0.848	0.015	0.015	0.0	0.002	0.0	1.759	2.200	
	44	0.0	0.231	0.779	0.017	0.015	0.0	0.0	0.0	1.673	2.282	
	42	0.0	0.178	0.828	0.012	0.014	0.0	0.002	0.0	1.732	2.227	
	46	0.0	0.234	0.784	0.014	0.015	0.0	0.0	0.0	1.682	2.274	
	47	0.001	0.228	0.785	0.016	0.017	0.0	0.0	0.011	1.691	2.257	Core
	56	0.0	0.187	0.824	0.016	0.013	0.0	0.0	0.0	1.720	2.237	Core
	57	0.0	0.194	0.813	0.016	0.013	0.0	0.0	0.0	1.730	2.233	close to dark incl.
	58	0.001	0.170	0.827	0.015	0.019	0.0	0.0	0.002	1.760	2.206	Outermost rim
	59	0.001	0.258	0.738	0.020	0.017	0.0	0.0	0.0	1.652	2.309	Small cryst.
910	198	0.001	0.187	0.836	0.016	0.015	0.0	0.0	0.0	1.750	2.207	Core
	199	0.001	0.152	0.882	0.012	0.013	0.0	0.002	0.0	1.761	2.185	
	200	0.001	0.156	0.870	0.012	0.015	0.0	0.0	0.0	1.756	2.195	Rim
	202	0.001	0.255	0.752	0.017	0.014	0.001	0.0	0.003	1.638	2.313	Core
	203	0.001	0.255	0.752	0.016	0.016	0.003	0.0	0.018	1.635	2.303	Rim
	204	0.001	0.226	0.788	0.017	0.016	0.0	0.0	0.0	1.704	2.255	Small
	205	0.0	0.195	0.825	0.015	0.013	0.0	0.0	0.002	1.716	2.236	Small
	209	0.001	0.190	0.822	0.016	0.014	0.0	0.0	0.0	1.700	2.252	Pheno
930	161	0.002	0.187	0.810	0.019	0.015	0.0	0.0	0.0	1.714	2.245	Rim
	162	0.001	0.175	0.828	0.018	0.012	0.0	0.0	0.0	1.734	2.227	
	163	0.001	0.196	0.800	0.025	0.015	0.0	0.010	0.0	1.713	2.237	Core
	164	0.0	0.183	0.815	0.025	0.014	0.0	0.009	0.0	1.719	2.229	Core
	165	0.0	0.171	0.813	0.017	0.012	0.0	0.0	0.0	1.742	2.230	Core
	166	0.001	0.173	0.824	0.017	0.014	0.0	0.0	0.0	1.749	2.218	Rim
	173	0.001	0.199	0.795	0.010	0.010	0.0	0.0	0.0	1.720	2.253	Core
? 174	175	0.001	0.232	0.756	0.010	0.011	0.0	0.0	0.0	1.687	2.288	Rim
	176	0.002	0.321	0.676	0.039	0.046	0.002	0.016	0.002	1.510	2.388	Groundmass
1020	212	0.0	0.168	0.843	0.017	0.013	0.0	0.006	0.0	1.748	2.204	Pheno
1100	178	0.001	0.257	0.725	0.017	0.015	0.002	0.0	0.0	1.647	2.322	Core
	179	0.001	0.263	0.734	0.020	0.016	0.0	0.0	0.0	1.622	2.332	
	180	0.0	0.189	0.801	0.016	0.015	0.0	0.0	0.0	1.748	2.225	
	181	0.001	0.201	0.791	0.020	0.018	0.0	0.004	0.0	1.719	2.242	Outermost rim
	182	0.001	0.172	0.821	0.015	0.013	0.0	0.0	0.0	1.738	2.229	Core
	183	0.001	0.185	0.824	0.017	0.014	0.0	0.0	0.0	1.735	2.224	
	184	0.001	0.157	0.826	0.014	0.014	0.0	0.0	0.0	1.753	2.219	Rim
	185	0.001	0.225	0.764	0.017	0.012	0.0	0.0	0.0	1.686	2.283	Core
	186	0.001	0.231	0.762	0.019	0.017	0.0	0.0	0.0	1.678	2.285	Rim

TABLE 8 – *Continued*

Bochum No.	Point	K	Na	Ca	Mg	Fe ²⁺	Mn	Ti	Cr	Al	Si	Remarks
1200	26	0.001	0.204	0.816	0.016	0.012	0.0	0.005	0.0	1.686	2.258	Core
	27	0.001	0.153	0.873	0.014	0.011	0.0	0.0	0.0	1.768	2.186	Rim
	30	0.001	0.193	0.835	0.014	0.012	0.002	0.0	0.0	1.720	2.230	Core
	31	0.0	0.189	0.832	0.015	0.013	0.0	0.0	0.0	1.734	2.222	
	33	0.0	0.196	0.831	0.016	0.015	0.0	0.0	0.0	1.700	2.245	
	34	0.0	0.177	0.834	0.023	0.013	0.002	0.013	0.002	1.724	2.212	
	35	0.0	0.187	0.835	0.016	0.011	0.0	0.0	0.0	1.715	2.236	
	36	0.0	0.187	0.834	0.015	0.013	0.0	0.0	0.0	1.719	2.233	
	37	0.0	0.210	0.823	0.017	0.013	0.0	0.0	0.0	1.700	2.246	Rim
	38	0.001	0.271	0.785	0.017	0.016	0.0	0.0	0.0	1.641	2.292	Rim, pheno
39	0.001	0.183	0.843	0.015	0.016	0.0	0.0	0.0	1.733	2.217	Pheno	
1280	63	0.002	0.304	0.695	0.023	0.030	0.0	0.004	0.0	1.573	2.366	Groundmass cryst.
1370	42	0.001	0.272	0.734	0.015	0.019	0.0	0.0	0.0	1.619	2.333	Pheno
	44	0.002	0.276	0.724	0.018	0.018	0.0	0.002	0.0	1.610	2.341	Pheno
	45	0.001	0.221	0.804	0.021	0.013	0.0	0.0	0.0	1.674	2.270	Core
	46	0.0	0.151	0.877	0.016	0.015	0.0	0.0	0.0	1.762	2.187	Rim

TABLE 9
Modal Analyses (%) of Selected Samples From Hole 396B

Bochum Sample No.	Plag.	Ol.	Glasses	Voids	Plag/ol.	Total (%)	Points Counted
600	15.6	1.3	83.0	0.1	12.0	100	2853
980	15.5	2.4	82.1	< 0.1	6.5	100.1	3615
1110	15.6	0.9	83.4	-	17.3	99.9	1957
1140	17.7	2.0	80.3	-	8.9	100	1955
1180	21.9	2.3	75.8	-	9.5	100	3687
860/870	17.3	2.9	79.5	0.3	6.0	100	2059
940	16.1	3.4	80.4	< 0.1	4.7	100	1920
1000	15.7	1.6	81.2	1.6	9.8	100.1	2301
1020	23.7	6.2	68.3	1.9	3.8	99.9	2273
1030	18.2	2.8	79.0	< 0.01	6.5	100.01	2369
1060	14.9	2.0	82.2	1.0	7.5	100.1	2152
1090	18.7	4.4	77.0	< 0.1	4.3	100.2	10,948
1360	14.5	1.7	83.8	< 0.1	8.5	100.1	1989
1370	8.1	2.2	89.4	< 1.0	3.7	100.7	2374

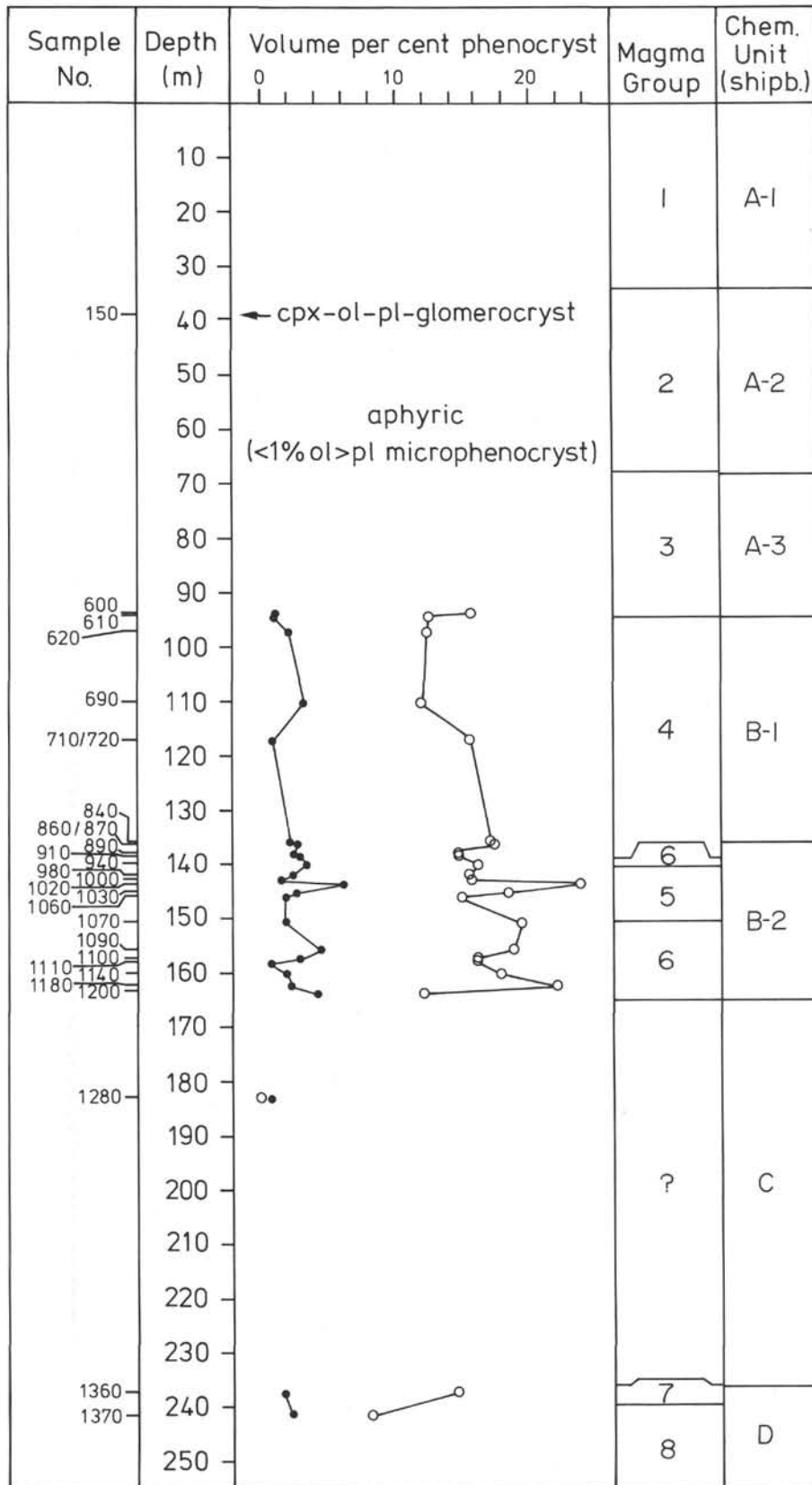


Figure 2. Volume per cent of olivine (●) and plagioclase (○) phenocrysts plotted with depth, for modally analyzed samples (see Table 9).

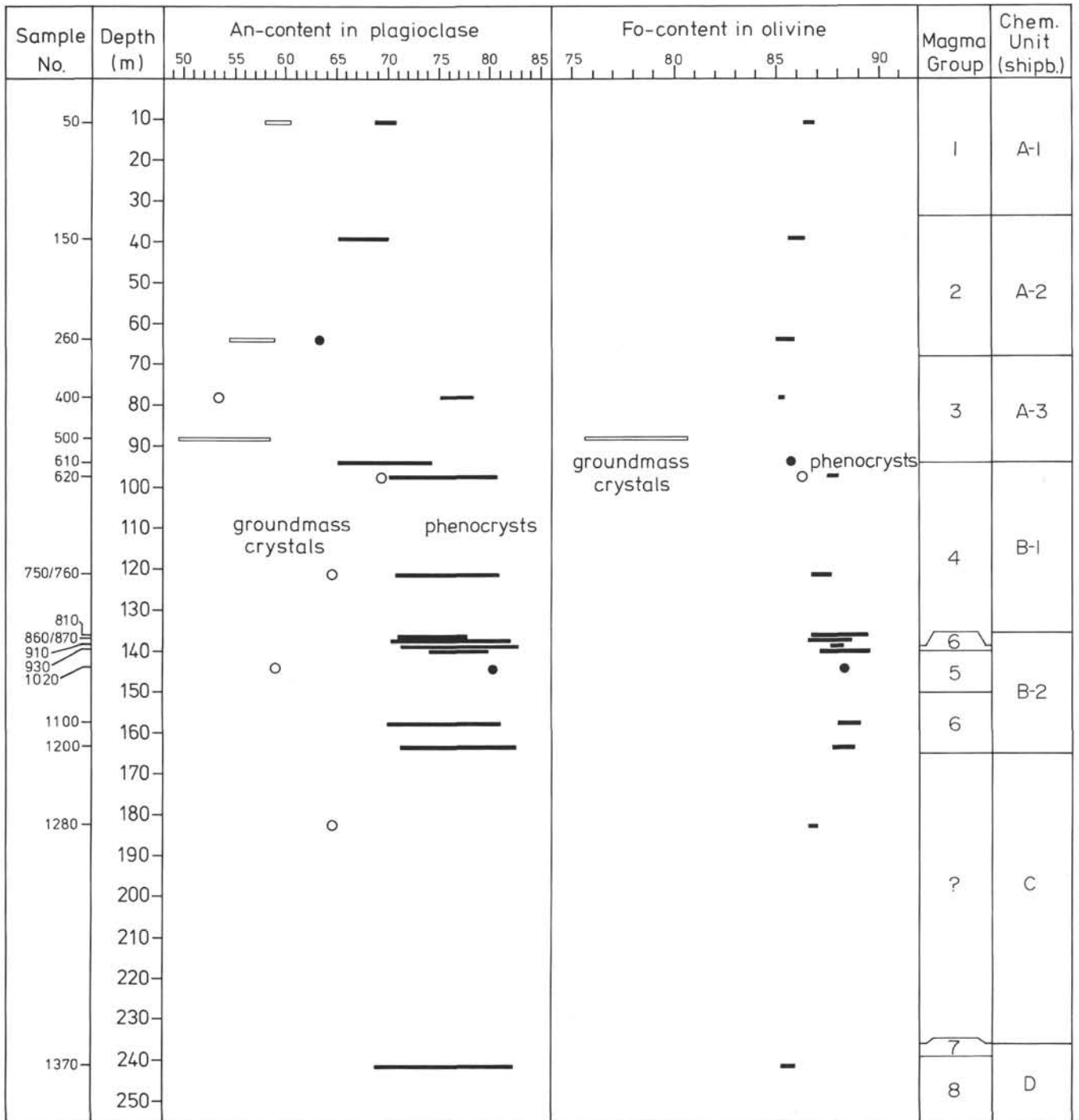


Figure 3. Ranges of plagioclase and olivine compositions for phenocrysts and groundmass crystals plotted with depth; data from electron microprobe analyses (see Tables 6 and 8).

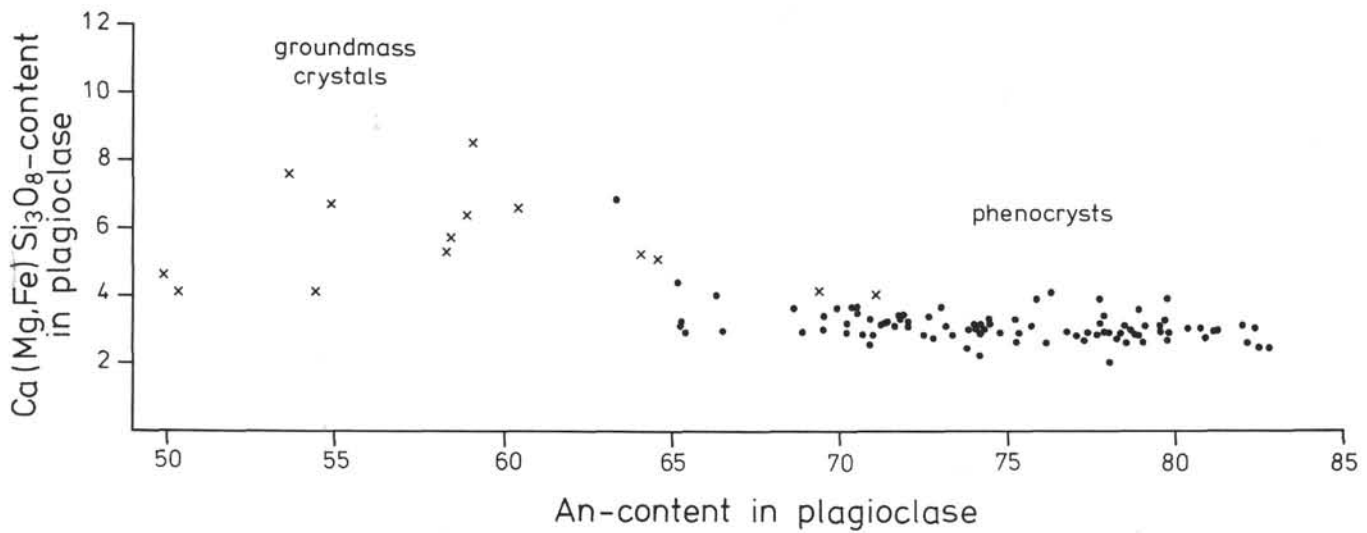


Figure 4. Molecular $Ca(Mg, Fe)Si_3O_8$ content in groundmass and phenocryst plagioclase plotted against anorthite; from electron microprobe data in Table 8.

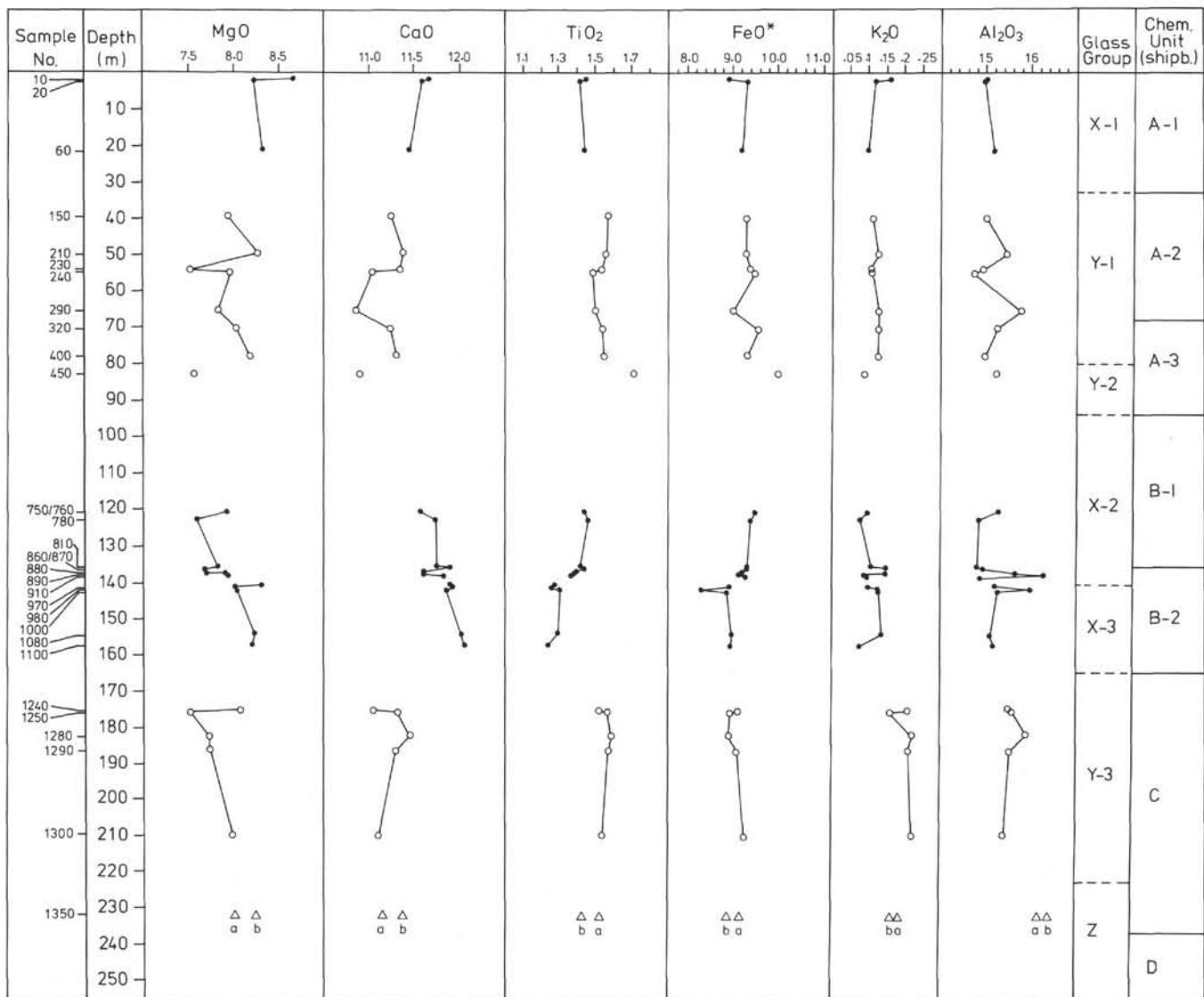


Figure 5. Plots of oxide contents for MgO, CaO, TiO₂, FeO (total Fe-oxide), K₂O, and Al₂O₃ versus sub-basement depth for glass compositions. Liquid types are indicated.

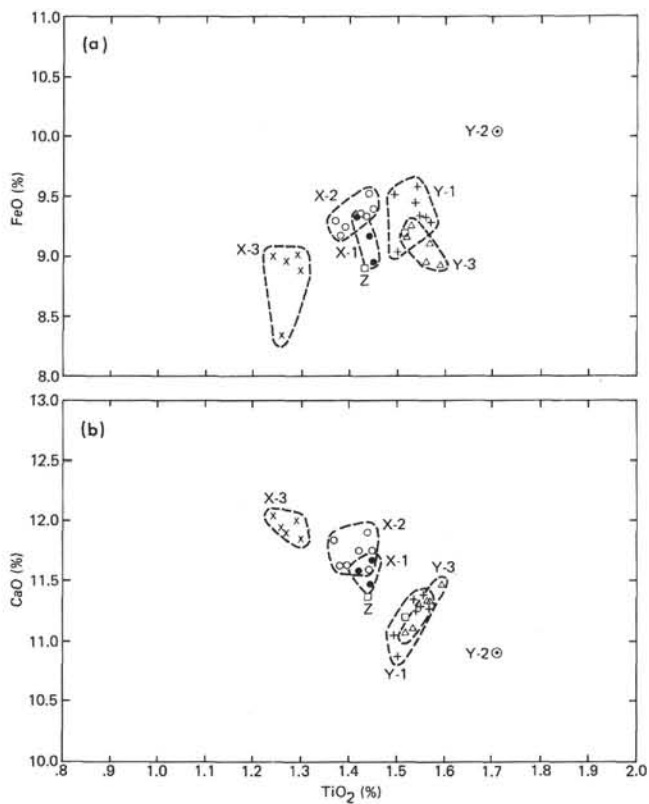


Figure 6. Plots of (a) FeO versus TiO₂, and (b) CaO versus TiO₂ for glass compositions; compositional-stratigraphic groups outlined.

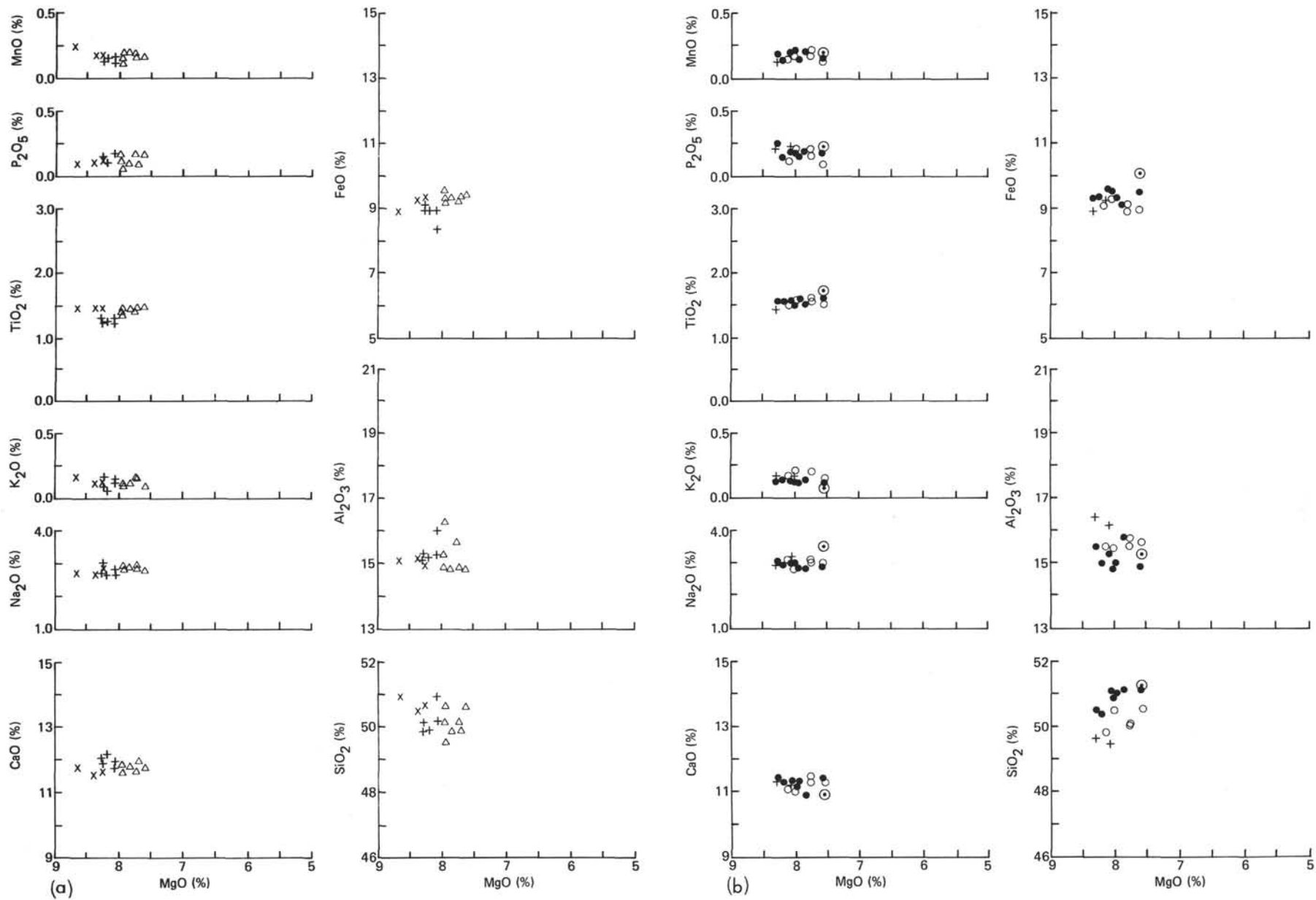


Figure 7. Oxide versus MgO variation for (a) X-type glasses and (b) Y-type and Z-type glasses; symbols: X-1 = x, X-2 = Δ , X-3 = +, Y-1 = \bullet , Y-2 = \circ , Y-3 = \circ , and Z = \oplus .

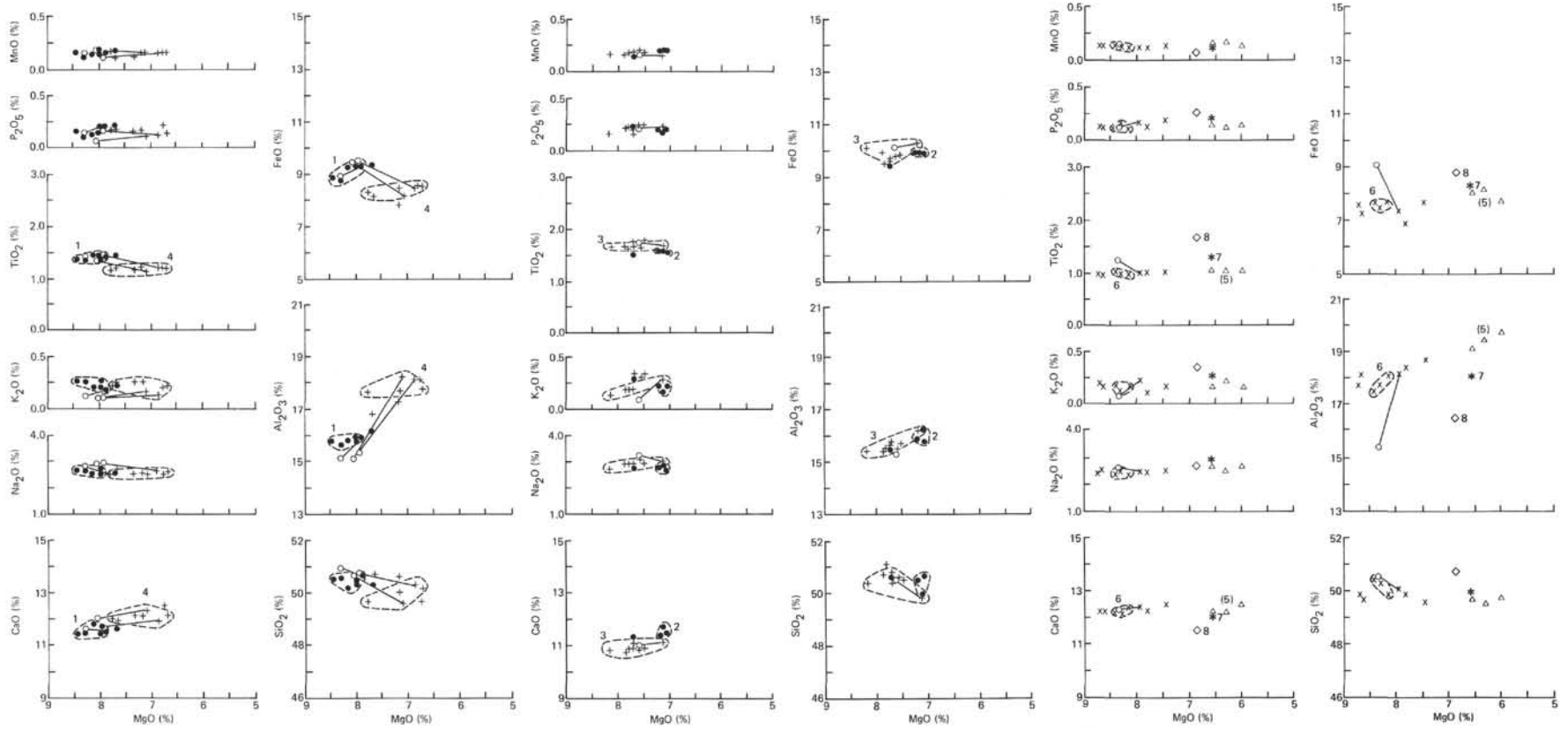


Figure 8. Oxide versus MgO variation for (a) magma batches 1-● and 4-+ (related to X-type liquids), (b) batches 2-● and 3-+ (related to Y-type liquids), and (c) batches 5-Δ and 6-x (related to X-type liquids), and 7-* and 8-◇ (probably Y-types). All analyses are corrected for carbonate (see text) and normalized to a H_2O^+ -free basis. Those with less than 1.25% H_2O^+ ("fresh" samples) are outlined in terms of respective groupings. Representative tie-lines have been drawn between whole rock and associated glass cooling rind compositions.

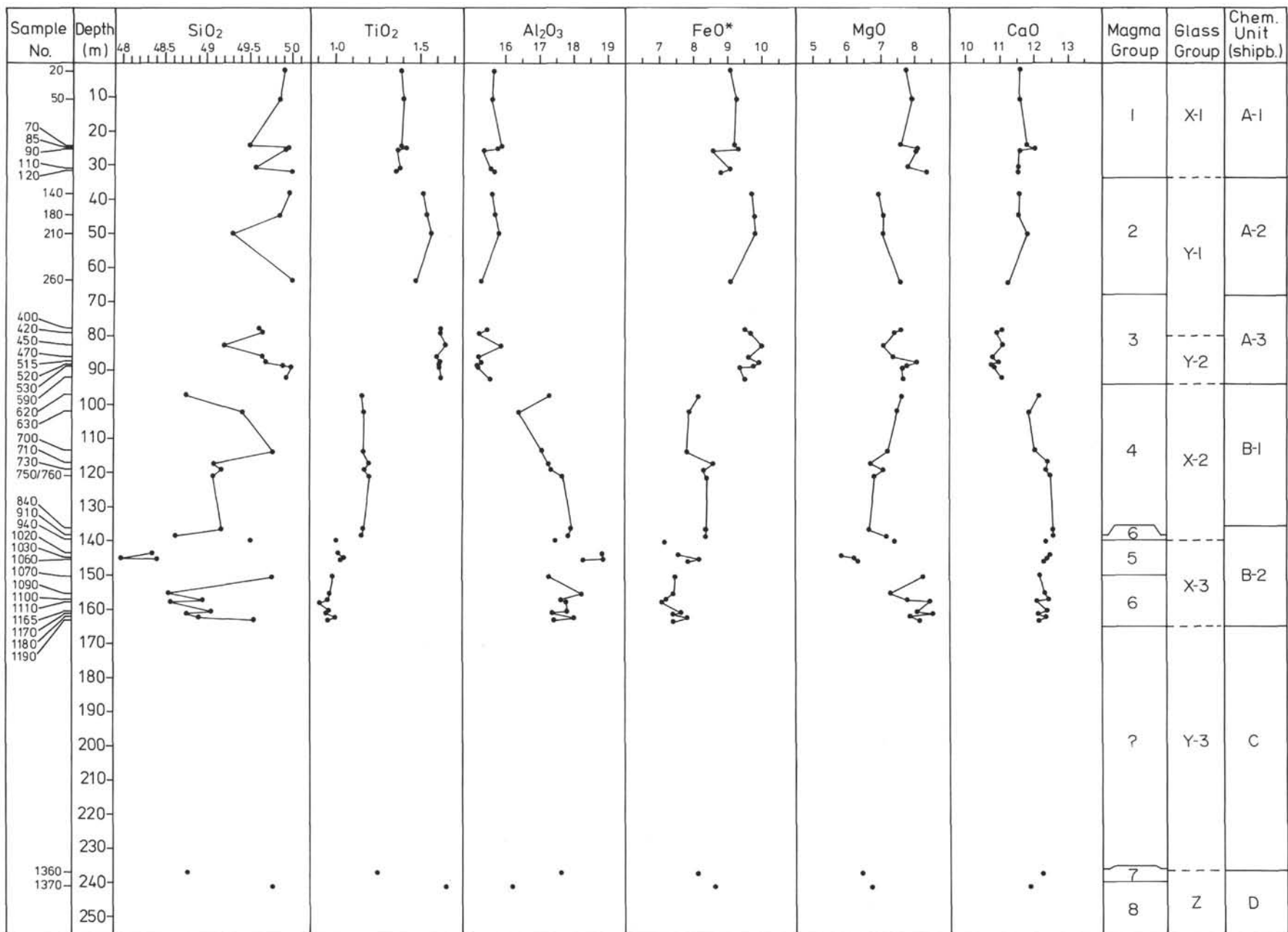


Figure 9a. Plots of major oxides versus sub-basement depth for whole-rock compositions. Magma groupings are indicated for their approximate stratigraphic occurrence. Plots of SiO₂, TiO₂, Al₂O₃, FeO (total iron), MgO, and CaO versus sub-basement depth.

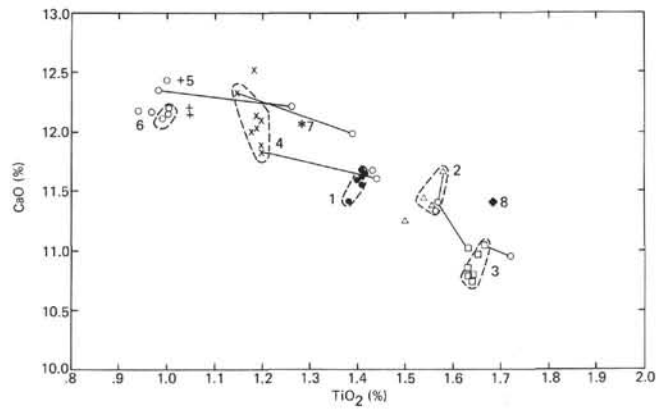


Figure 10. CaO versus TiO_2 for whole rock compositions, carbonate-corrected and normalized to a H_2O^+ -free basis. Tie-lines drawn to associated glass cooling rind compositions; magma batches 1 = ●, 2 = △, 3 = □, 4 = x, 5 = +, 6 = ○, 7 = *, and 8 = ◆, outlined for samples with 1.25% H_2O^+ .

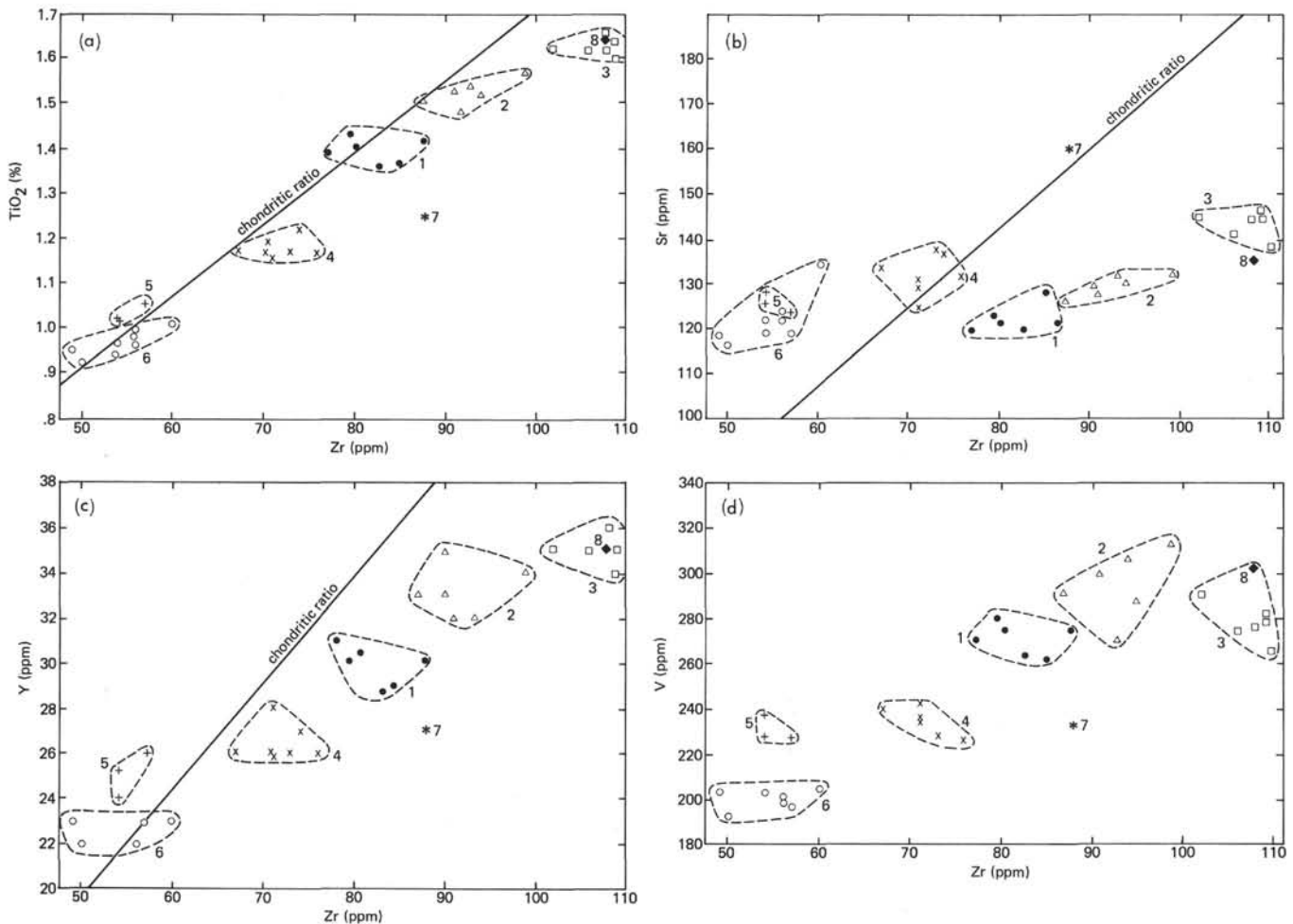


Figure 11. Plots of large ion lithophile elements versus Zr: (a) TiO_2 , (b) Y, (c) Sr, (d) V; magma batches are outlined (chondritic Ti/Zr av. ≈ 103 , Leg 46 range: 107 to 92 [X-3 to Y-2]; chondritic Y/Zr av. ≈ 0.43 , Leg 46 range: 0.46 to 0.32 [X-3 to Y-2]; chondritic Sr/Zr av. ≈ 2.8 , Leg 46 range: 2.8 to 1.3 [X-3 to Y-2]; and chondritic V/Zr av. ≈ 12 , Leg 46 range: 4.2 to 2.6 [X-3 to Y-2]).

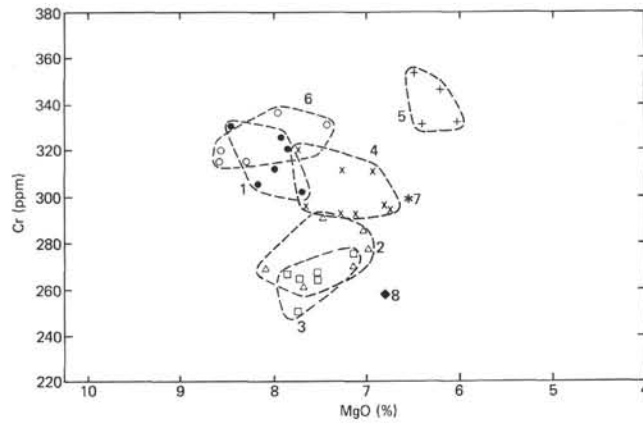


Figure 12. Plots of Cr versus MgO with postulated magma batches outlined. Magma batch 1 = ●, 2 = △, 3 = □, 4 = ×, 5 = +, 6 = ○, 7 = *, and 8 = ◆.

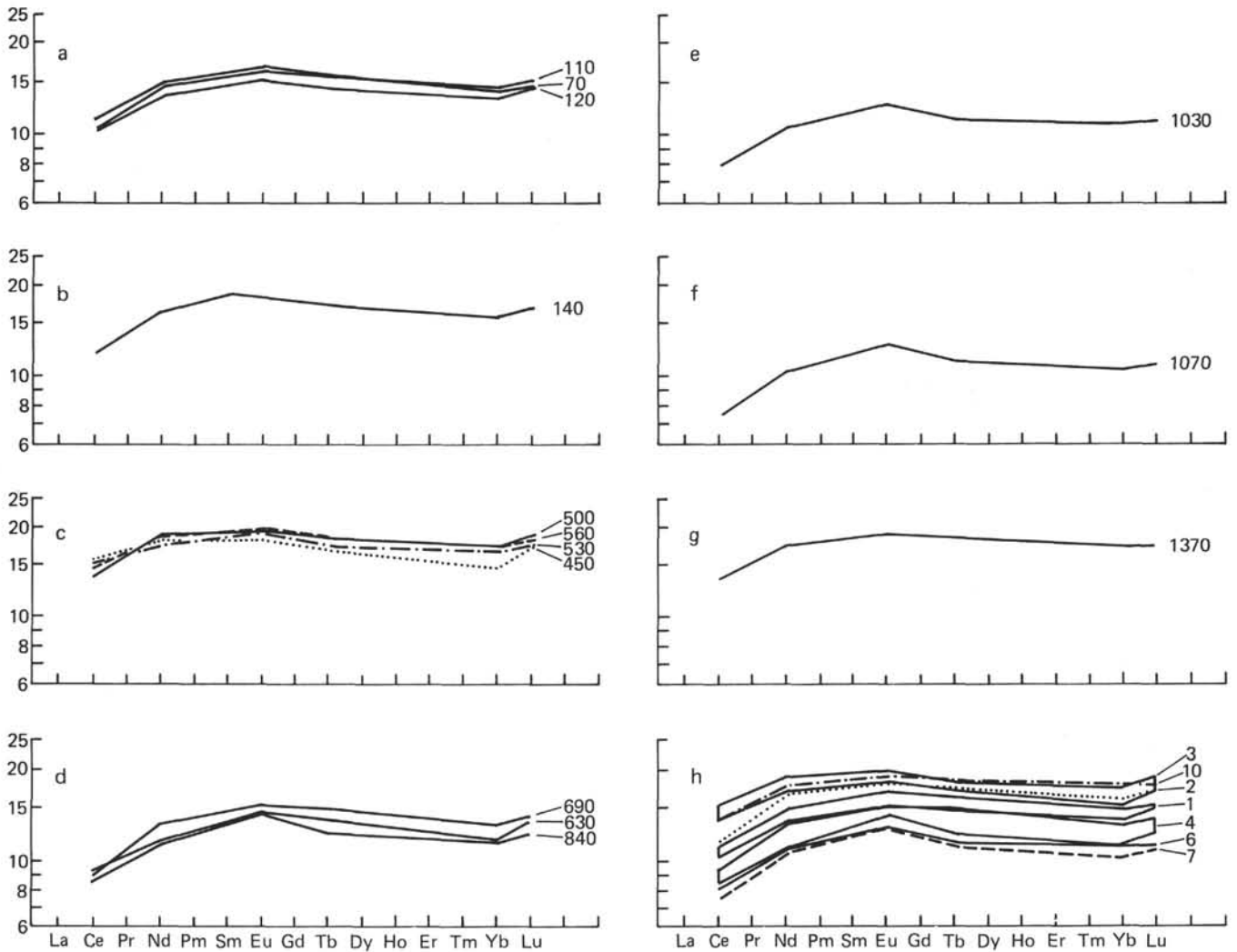


Figure 13. Plots of chondrite-normalized rare earth element abundances, with increasing rare earth atomic number, according to magma batches: (a) 1, (b) 2, (c) 3, (d) 4, (e) 5, (f) 6, and (g) 8, and in (h) a summary for the respective magma batch ranges.

PLATE 1

- Figure 1 Olivine-Plagioclase-Clinopyroxene glomerocryst.
Bochum Sample 150; DSDP Sample 396B-8-2, 3-7
cm. O = Olivine, C = Clinopyroxene.
- Figure 2 Plagioclases. Bochum Sample 610; DSDP Sample
396B-15-5, 108-111 cm.
- Figure 3 Plagioclases. Bochum Sample 1110; DSDP Sample
396B-22-2, 8-12 cm.
- Figure 4 Plagioclases. Bochum Sample 700; DSDP Sample
396B-16-5, 34-36 cm.

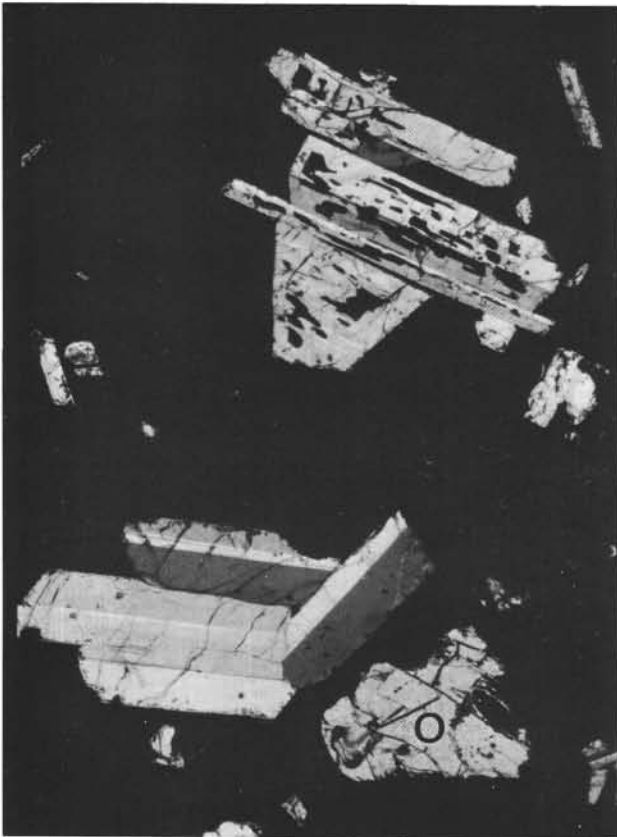
PLATE 1



1 0.5 mm



2 1 mm



3 0.5 mm

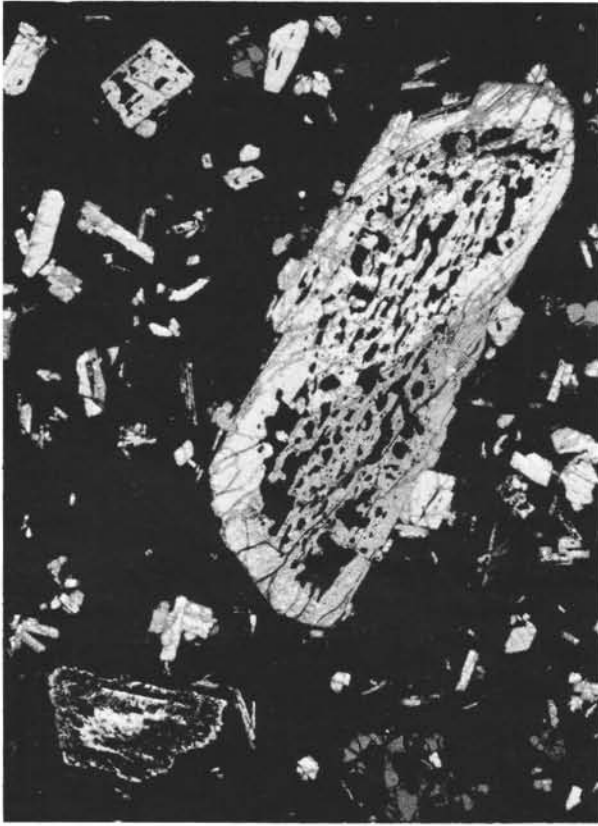


4 1 mm

PLATE 2
Plagioclases

- Figure 1 Bochum Sample 1170; DSDP Sample 396B-22-3,
49-56 cm.
- Figure 2 Bochum Sample 860/870; DSDP Sample 396B-20-1,
70-80 cm.
- Figure 3 Bochum Sample 600; DSDP Sample 396B-15-5,
102-105 cm.
- Figure 4 Bochum Sample 910; DSDP Sample 396B-20-2,
58-67 cm.

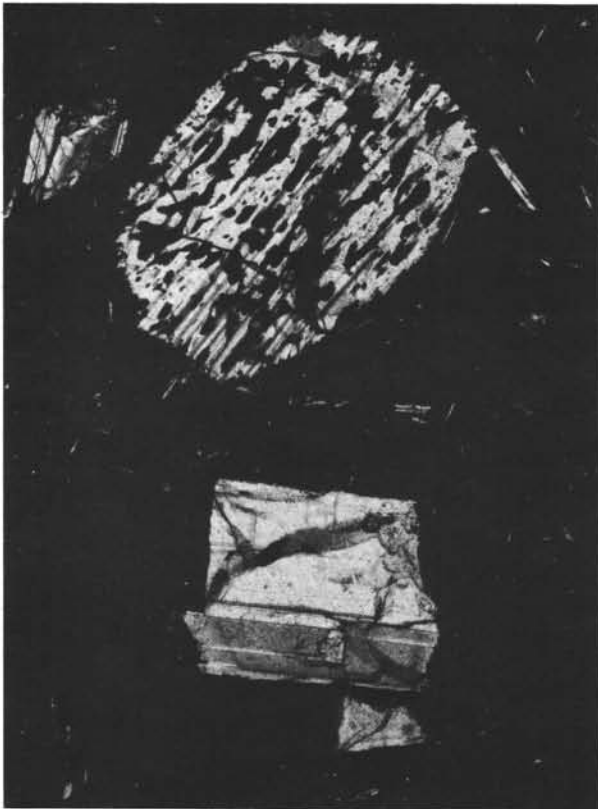
PLATE 2



2 mm



1 mm



0.5 mm



0.5 mm

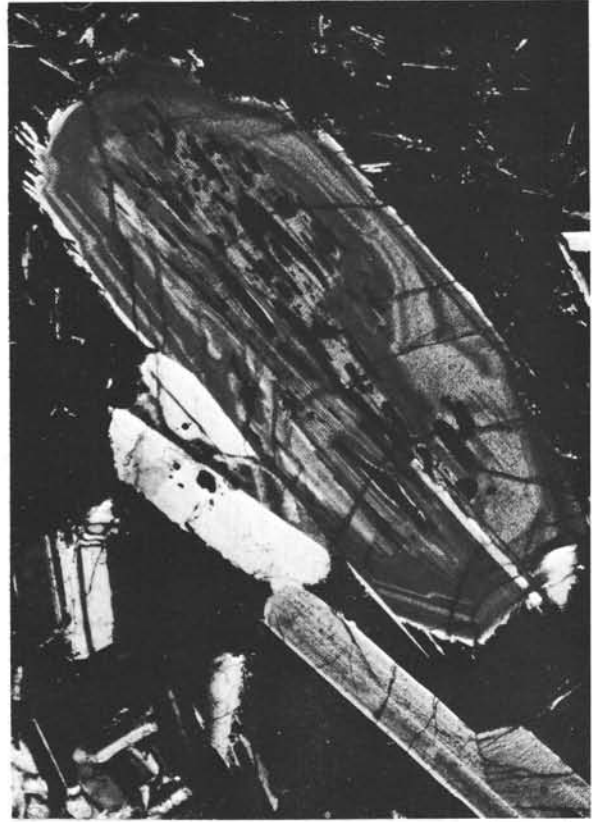
PLATE 3
Plagioclases

- Figure 1 Bochum Sample 840; DSDP Sample 396B-20-1,
35-42 cm.
- Figure 2 Bochum Sample 710/720; DSDP Sample 396B-17-1,
4-7 cm.
- Figure 3 Bochum Sample 1100; DSDP Sample 396B-22-1,
125-134 cm.
- Figure 4 Bochum Sample 1100; DSDP Sample 396B-22-1,
125-134 cm.

PLATE 3



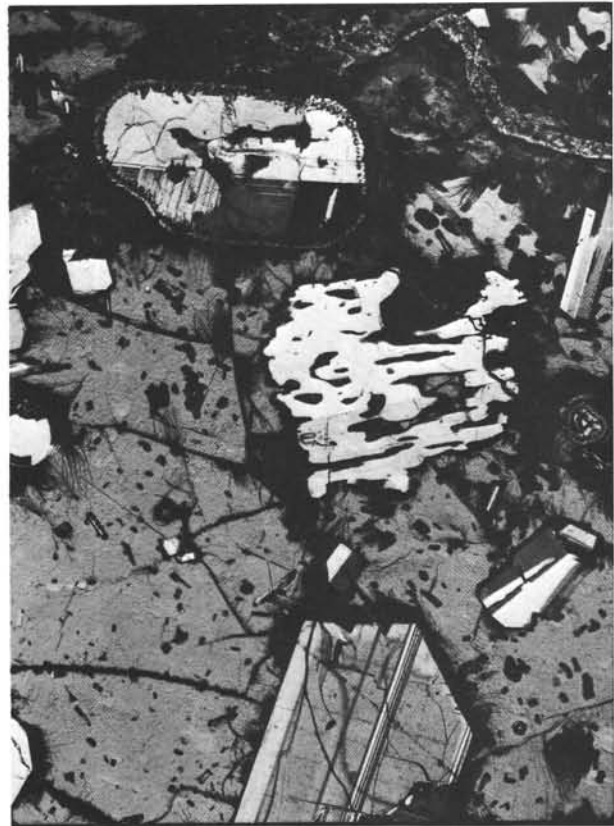
0.5 mm



0.25 mm



0.3 mm



0.5 mm

PLATE 4
Plagioclases

- Figure 1 Bochum Sample 50; DSDP Sample 396B-5-2, 87-98
 cm. O = Olivine.
- Figure 2 Bochum Sample 160; DSDP Sample 396B-8-3, 25-30
 cm.
- Figure 3 Bochum Sample 400; DSDP Sample 396B-14-1,
 121-127 cm.
- Figure 4 Bochum Sample 780; DSDP Sample 396B-18-1,
 22-27 cm.

PLATE 4

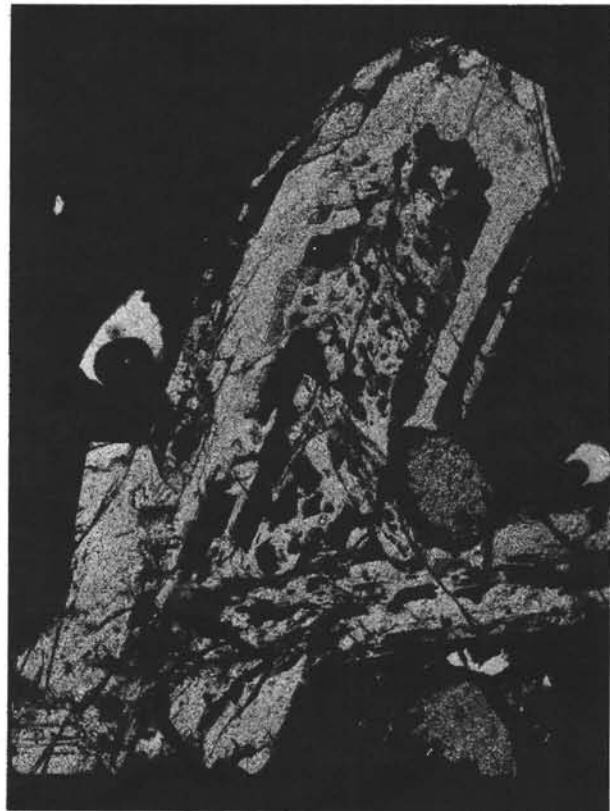


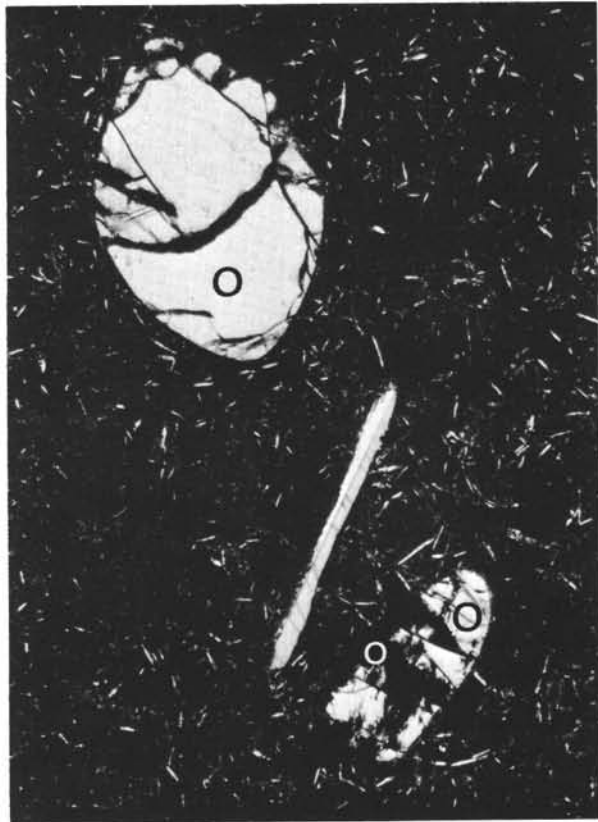
PLATE 5
Olivines

- Figure 1 Bochum Sample 860/870; DSDP Sample 396B-20-1,
70-80 cm.
- Figure 2 Bochum Sample 260; DSDP Sample 396B-11-2,
27-33 cm. O = Olivine.
- Figure 3 Bochum Sample 860/870; DSDP Sample 396B-20-1,
70-80 cm.
- Figure 4 Bochum Sample 1370; DSDP Sample 396B-32-1,
59-62 cm.

PLATE 5



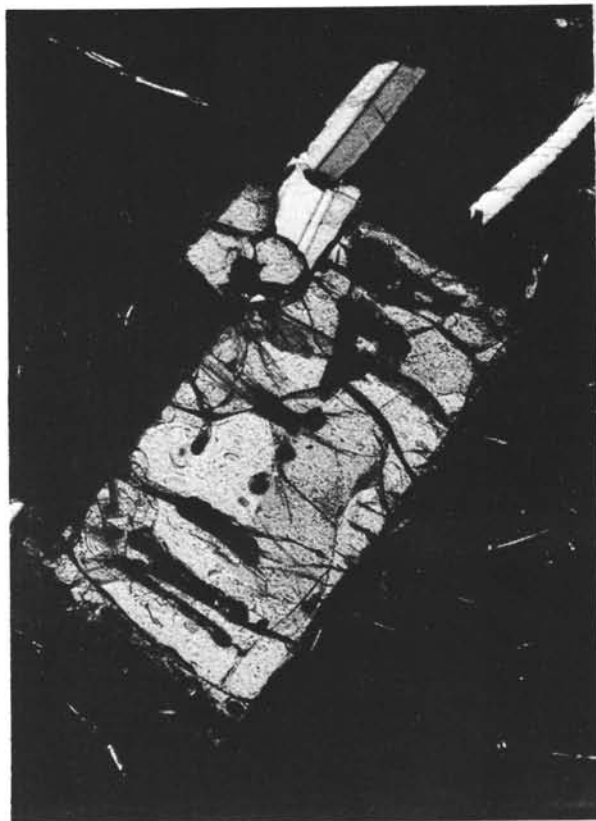
0.5 mm



0.5 mm



1 mm



0.2 mm